Euro. Jnl of Applied Mathematics (2006), *vol.* 17, *pp.* 347–382. © 2006 Cambridge University Press
doi:10.1017/S0956792506006589 Printed in the United Kingdom

On a model for the motion of a contact line on a smooth solid surface

J. BILLINGHAM

School of Mathematical Sciences, University of Nottingham, University Park, Nottingham NG7 2RD, UK
email: John.Billingham@Nottingham.ac.uk

(*Received 8 June 2005; revised 28 March 2006*)

In this paper we investigate the model for the motion of a contact line over a smooth solid surface developed by Shikhmurzaev, [24]. We show that the formulation is incomplete as it stands, since the mathematical structure of the model indicates that an additional condition is required at the contact line. Recent work by Bedeaux, [4], provides this missing condition, and we examine the consequences of this for the relationship between the contact angle and contact line speed for Stokes flow, using asymptotic methods to investigate the case of small capillary number, and a boundary integral method to find the solution for general capillary number, which allows us to include the effect of viscous bending. We compare the theory with experimental data from a plunging tape experiment with water/glycerol mixtures of varying viscosities [11]. We find that we are able to obtain a reasonable fit using Shikhmurzaev's model, but that it remains unclear whether the linearized surface thermodynamics that underlies the theory provide an adequate description for the motion of a contact line.

1 Introduction

More than ten years ago, Shikhmurzaev introduced a theory that provides a model for the motion of a contact line over a smooth solid surface [24]. The model has a number of attractive features:

(1) Since the theory is based on a simple model for the thermodynamics of the fluid close to interfaces, its main components can be derived without any reference to contact lines, and indeed has proved to be of use in situations where no contact line is present, for example, in modelling cusps, the coalescence of liquid droplets and the break up of liquid threads [28, 29, 31].

(2) The dynamic contact angle is determined as part of the solution. No empirical correlation is needed.

(3) The stress singularity at the contact line that arises as a result of the usual no slip boundary condition [13], is eliminated by introducing slip, not in an ad hoc manner, but as a consequence of the thermodynamics of the fluid/solid interface.

(4) The theory leads naturally to a flux of fluid through the contact line, as is observed experimentally [13]. Most other models lead to a sliding motion.

https://doi.org/10.1017/S0956792506006589 Published online by Cambridge University Press

(5) The theory has the potential to explain the phenomenon of 'hydrodynamic assist of wetting' whereby the dynamic contact angle is a function of both the contact line velocity *and* the flow field [9, 10].

(6) Results derived using the theory are in good agreement with experimental results for steady Stokes flow [24, 27].

In this paper, we will demonstrate that, in spite of these features, the theory is incomplete as it stands.

It is not our intention either to give a complete defence of the assumptions that underlie the theory, or to give an overview of the other theories that have been put forward as models for the motion of contact lines, for example, [21]. These issues have been addressed at length in a series of papers by Shikhmurzaev over the past ten years, and we refer the reader in particular to earlier work [14, 27, 32].

We begin in section 2 by informally discussing some of the key features of Shikhmurzaev's theory and writing down the governing equations. We then eliminate all of the surface variables except for the surface density and bulk fluid velocity. This allows us to see that the surface density satisfies a nonlinear diffusion equation forced by the flow. It then becomes clear that, in order to determine the contact angle and provide connection conditions for the two nonlinear, second order equations for the surface densities at the free surface and the solid surface, three conditions are required at the contact line, not just the two proposed by Shikhmurzaev. The appropriate additional condition was recently derived by Bedeaux [4]. In § 3 we consider how the theory works for the case of Stokes flow in a wedge with strong surface tension (small capillary number), and show how the original analysis [24, 26], does not account for a one parameter family of solutions, which exists in the absence of the third condition at the contact line. In § 4 we solve the full equations numerically using a boundary integral method, so that we can assess the additional effect of viscous bending on the free surface. This also allows us to confirm that the asymptotic solution we developed in § 3 is consistent with numerical solutions when the capillary number, Ca, is sufficiently small. In § 5, we compare the relationship between the contact angle and contact line speed implied by this new condition with some experimental data. It is worth noting that, of the six features of the theory listed above, only number 6 needs to be reconsidered in the light of this new development. We will find that by including the missing boundary condition at the contact line and the effect of viscous bending of the free surface, we are able to fit the model, which now involves seven dimensionless parameters, to the experimental data and estimate the material parameters associated with the surface layers. The resulting estimates for some of the parameters do not agree well with the order of magnitude estimates that we expect to characterize them. In § 6, we make some suggestions as to how the theory might be modified, and describe another experiment that could resolve some of the remaining questions about the theory.

2 An overview of Shikhmurzaev's theory

Consider a static contact line, as shown in Figure 1. If the surface tensions associated with the interfaces between fluids 1 and 2 and the solid surface are σ_{12}, σ_{1S} and σ_{2S}, the

https://doi.org/10.1017/S0956792506006589 Published online by Cambridge University Press

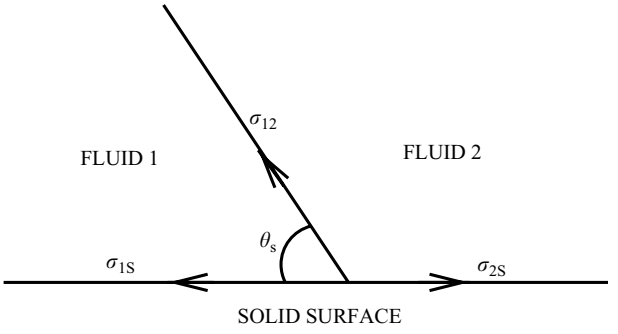


FIGURE 1. The forces that act at a static contact line.

horizontal force balance is given by the Young–Laplace equation,

$$\sigma_{12}\cos\theta_s + \sigma_{1S} = \sigma_{2S}. \tag{2.1}$$

Since the surface tension forces act upon a line, which has no mass, and because the flux of momentum at the contact line is negligible, (2.1) also holds when the contact line is moving [4, 24, 33]. Bending of the interface by viscous forces very close to the contact line leads to a difference between the apparent contact angle, θ_{app}, which can be measured experimentally, and the actual, or microscopic, dynamic contact angle, θ_c. However, experimental observations show that θ_c itself also varies with the velocity of the contact line [12]. This means that at least one of σ_{12}, σ_{1S} and σ_{2S} must deviate from its static value when the contact line is moving.

An examination of the flow field close to a moving contact line gives a straightforward explanation of this phenomenon [13]. Fluid molecules are advected along the free surface, where they are in a thermodynamic state associated with the surface tension σ_{12}, through the contact line and into the interface between the fluid and the solid surface, where their *equilibrium* thermodynamic state is associated with the surface tension σ_{1S}. However, the fluid molecules take a finite time to relax from the state associated with σ_{12} to that associated with σ_{1S}. The surface tension of the interface between the fluid and the solid surface will therefore be different from the static value, σ_{1S}, in some neighbourhood of the contact line and, in particular, the value at the contact line, which we must use in (2.1), will be different from σ_{1S}. This leads to a dynamic contact angle different from the static value. This simple idea is the basis of Shikhmurzaev's theory.

A consequence of the gradient in surface tension close to the contact line is that the classical no slip boundary condition is modified so that there is an *apparent* slip between the bulk fluid and the solid surface, in a sense that we shall discuss more fully below. As a result, the force on the solid surface is bounded [24]. In this way, the two major modelling difficulties associated with moving contact lines, namely the specification of θ_c as a function of the velocity of the contact line, and the modification of the no slip boundary condition, are dealt with in a simple, consistent theory derived from first principles. However, we shall see later that, although the force on the solid surface certainly is bounded, the singularity is not relieved in quite the manner suggested elsewhere [24].

We now need to examine some of the details of the theory. Consider the interface between a liquid and another immiscible liquid, a gas or a solid surface. The liquid

https://doi.org/10.1017/S0956792506006589 Published online by Cambridge University Press

molecules close to the interface experience an asymmetric force due to the presence of the other material. This results in a slightly different liquid density in a thin surface layer, typically $h \approx 10^{-10}$ m thick. This is what gives rise to the surface tension, σ. Note that when we refer to h, we should think of it as an order of magnitude estimate that we can use to estimate the sizes of some of the other parameters, not as a well-defined layer thickness, since the layer thickness does not appear explicitly in the theory. We can define the surface density to be the integral of the liquid density across the layer[1]. The surface can then be treated as a thermodynamic system characterised by temperature and surface density, which exists at the surface of the bulk fluid. As pointed out by Shikhmurzaev [24], this is the structureless approach to modelling the surface phase, which is appropriate when the lengthscale of the bulk flow is much greater than h, so that the surface phase has, asymptotically, zero thickness, and simply modifies the boundary conditions for the bulk flow.

For isothermal flows we can treat the surface tension, σ, as a function of the local surface density only. Since we do not expect very large changes in surface density, it is simplest to assume that the surface tension varies linearly with the surface density, so that

$$\sigma = \gamma(\rho_{0s} - \rho_s). \tag{2.2}$$

Both γ and ρ_{0s} are constants that must be determined experimentally. In principle, this could be an experiment that has nothing to do with contact lines. We are not, however, completely in the dark about the magnitude of these constants. The surface layer density is close to the bulk density. For water, where $\rho \approx 1000$ kg m^{-3}, this means that $\rho_{0s} \approx h\rho \approx 10^{-7}$ kg m^{-2}. The compressibility of the surface layer will be similar to that of the bulk fluid, so that, for water, $\gamma \approx 2 \times 10^6$ m^2 s^{-2}.

The next step is to consider the dynamics of the liquid that forms the surface layer. We can define a surface layer velocity, $\mathbf{v}_s$, so that $\rho_s \mathbf{v}_s$ is the flux of mass in the surface layer, and conservation of mass can be written as

$$\frac{\partial \rho_s}{\partial t} + \nabla_s \cdot (\rho_s \mathbf{v}_s) = -\frac{\rho_s - \rho_{es}}{\tau}. \tag{2.3}$$

Here ∇_s is the gradient operator restricted to the surface. If the right hand side of this equation were equal to zero, this would be the usual equation for conservation of mass. The actual right hand side represents a source of fluid that tends to drive the surface density towards its equilibrium value, ρ_{es}, over a time scale τ. This source of fluid consists of a flow of molecules from the bulk that is too weak to significantly affect the bulk fluid velocity[2], but which does affect the surface density. Note that (2.2) and (2.3) show that the equilibrium surface tension is $\sigma_e = \gamma(\rho_{0s} - \rho_{es})$.

Having written down equations for what goes on in the surface layer, we can now consider how this affects the bulk flow. This is governed by the usual Navier–Stokes

[1] The conventional way of treating the surface density is to use the equimolar surface as the dividing surface between the two phases and define an excess density [23, 14, 32]. Whether Shikhmurzaev's definition of surface density is consistent from the point of view of non-equilibrium surface thermodynamics, as discussed in Bedeaux *et al.* [3], is outside the scope of the present paper.

[2] See Shikhmurzaev [31] for a modification of the theory that takes into account the effect of this flux on the normal velocity.

https://doi.org/10.1017/S0956792506006589 Published online by Cambridge University Press

equations for an incompressible, Newtonian fluid,

$$\nabla \cdot \mathbf{u} = 0, \quad \rho \left(\frac{\partial \mathbf{u}}{\partial t} + \mathbf{u} \cdot \nabla \mathbf{u} \right) = -\nabla p + \mu \nabla^2 \mathbf{u}, \tag{2.4}$$

where $\mathbf{u}$ is the bulk velocity field and μ the bulk viscosity. We have assumed that the effect of gravity is negligible. The behaviour of the surface layer only affects the bulk flow through appropriate boundary conditions. Focussing on a liquid/solid interface for the moment, the first boundary condition is

$$2\mu \mathbf{n} \cdot \mathbf{e} \cdot (\mathbf{I} - \mathbf{nn}) + \frac{1}{2} \nabla_s \sigma = \beta \, (\mathbf{u} - \mathbf{U}) \cdot (\mathbf{I} - \mathbf{nn}), \tag{2.5}$$

where $\mathbf{n}$ is the outward unit normal, $\mathbf{I}$ is the unit tensor, $\mathbf{e} = \frac{1}{2} \left(\nabla \mathbf{u} + (\nabla \mathbf{u})^T \right)$ is the rate of strain tensor and $\mathbf{U}$ is the velocity of the solid surface[3]. Note that $2\mu \mathbf{n} \cdot \mathbf{e} \cdot (\mathbf{I} - \mathbf{nn})$ is the shear stress exerted on the interface by the bulk fluid and $(\mathbf{u} - \mathbf{U}) \cdot (\mathbf{I} - \mathbf{nn})$ is the tangential component of the difference between the bulk velocity and the solid surface velocity. Shikhmurzaev derived this, and the other boundary conditions that we shall discuss, by considering the equation for conservation of energy in the surface layer, applying the principles of near equilibrium thermodynamics, and seeking conditions that minimise the rate of production of entropy [3].

If the left hand side of (2.5) is nonzero, there *appears* to be slip between the bulk fluid and the solid. The fluid in the solid-facing side of the surface layer moves with the solid surface, whilst the fluid in the bulk-facing side of the surface layer can move at a different velocity. However, recall that, within the context of the structureless approach to modelling the surface layer, adopted here, the surface layer has zero thickness and affects the flow only through the boundary conditions. Equation (2.5) shows that both the shear stress exerted by the bulk fluid and gradients in surface tension can cause this apparent slip. The coefficient of sliding friction, β, is a constant with dimensions of viscosity divided by length, and has typical magnitude μ/h.

Three more boundary conditions are needed to complete the model for the solid surface layer. Firstly,

$$\mathbf{v}_s \cdot \mathbf{n} = \mathbf{u} \cdot \mathbf{n} = \mathbf{U} \cdot \mathbf{n}, \tag{2.6}$$

which simply states that the normal components of all three velocities are equal at the surface, and secondly,

$$\mathbf{v}_s \cdot (\mathbf{I} - \mathbf{nn}) = \frac{1}{2} (\mathbf{u} + \mathbf{U}) \cdot (\mathbf{I} - \mathbf{nn}) + \alpha \nabla_s \sigma. \tag{2.7}$$

If there were no surface tension gradient term in this equation, it would simply state that the tangential component of the surface layer velocity is the average of the tangential components of the bulk and interfacial velocities. The surface tension gradient term modifies this relationship in a manner analagous to ordinary fluid flow in a channel with

[3] Note that in steady moving contact line problems, it is usually convenient to work in a frame of reference where the contact line is fixed and the solid surface is moving.

https://doi.org/10.1017/S0956792506006589 Published online by Cambridge University Press

a pressure gradient[4]. The final constant, α, has dimensions of length divided by viscosity, and has a typical magnitude h/μ.

At a free surface, we have the usual conditions of continuity of normal and tangential stress at the free surface, taking into account the fact that the surface tension may vary along the interface. These are

$$-p + 2\mu \mathbf{n} \cdot \mathbf{e} \cdot \mathbf{n} = \sigma\kappa, \tag{2.8}$$

where $\kappa = \nabla \cdot \mathbf{n}$ is the curvature of the interface, and

$$2\mu \mathbf{n} \cdot \mathbf{e} \cdot (\mathbf{I} - \mathbf{nn}) = -\nabla_s \sigma. \tag{2.9}$$

Equation (2.9) states that gradients in surface tension cause a shear stress (a Marangoni stress) on the interface. Normal components of the the bulk and surface layer velocities must be continuous, (2.6), and also

$$\nabla_s \sigma = -\frac{4\beta}{1 + 4\alpha\beta} (\mathbf{u} - \mathbf{v_s}) \cdot (\mathbf{I} - \mathbf{nn}). \tag{2.10}$$

Equation (2.10) can be derived by eliminating $\mathbf{U} \cdot (\mathbf{I} - \mathbf{nn})$ between (2.5) and (2.7), and making use of (2.9). This completes the model for the surface layers. Note that we have yet to mention contact lines in the formulation.

When a liquid moves across a flat, smooth solid surface displacing a gas (which we shall initially treat as a void), a free surface and a liquid/solid surface, characterized by the above equations, meet at a contact line. From this point onwards, we will assume steady, two-dimensional flow in a frame of reference where the contact line is stationary, in which case the surface gradient operators above can be replaced with d/ds or d/ds_i, where s and s_i are arc length along the solid and free surfaces respectively. Since in this case $\mathbf{u} \cdot \mathbf{n} = \mathbf{v}_s \cdot \mathbf{n} = \mathbf{U} \cdot \mathbf{n} = 0$, it is convenient to write the tangential components of the bulk velocity at the interface, the surface layer velocity and the solid surface velocity as u_s, v_s and U respectively, measured in the direction of increasing s. We will use a superscript i for free surface layer quantities, and no superscript for solid surface layer quantities. In Shikhmurzaev [24], it is postulated that there are two conditions at the contact line: firstly, conservation of mass,

$$\rho_s^i v_s^i + \rho_s v_s = 0, \tag{2.11}$$

so that the amount of fluid that flows into the contact line from one layer flows out in the other layer, and secondly, conservation of momentum, which is just the horizontal force balance given by the Young–Laplace equation, (2.1), which becomes

$$\left(\rho_s^i - \rho_{0s}^i\right) \cos\theta_c = \left(\rho_{es}^i - \rho_{0s}^i\right) \cos\theta_s + \rho_{es} - \rho_s. \tag{2.12}$$

To clarify the structure of the model, we now eliminate the surface velocities and surface tensions, so that only the surface densities appear. Recall that these are assumed to be linearly related to the surface tensions through $\sigma = \gamma(\rho_{0s} - \rho_s)$. On the free surface, (2.3)

[4] A surface layer pressure can consistently be defined to be minus the surface tension, but, for clarity, we avoid using this concept here.

https://doi.org/10.1017/S0956792506006589 Published online by Cambridge University Press

and (2.10) become

$$\frac{d}{ds_i}\left(\rho_s^i v_s^i\right) + \frac{\rho_s - \rho_{es}}{\tau} = 0, \quad \frac{d\sigma^i}{ds_i} = -\gamma\frac{d\rho_s^i}{ds_i} = -\frac{4\beta}{1+4\alpha\beta}\left(u_s^i - v_s^i\right),$$

so that, upon eliminating v_s^i, we obtain

$$\frac{\gamma\alpha(1+4A)}{4A}\frac{d}{ds_i}\left(\rho_s^i\frac{d\rho_s^i}{ds_i}\right) - \frac{d}{ds_i}\left(\rho_s^i u_s^i\right) - \frac{\rho_s^i - \rho_{es}^i}{\tau} = 0, \tag{2.13}$$

where $A = \alpha\beta$ is a dimensionless constant[5]. In a similar manner, we obtain

$$2\mu\mathbf{n}\cdot\mathbf{e}\cdot(\mathbf{I}-\mathbf{nn}) = \gamma\frac{d\rho_s^i}{ds_i}, \tag{2.14}$$

$$-p + 2\mu\mathbf{n}\cdot\mathbf{e}\cdot\mathbf{n} = -\gamma\left(\rho_s^i - \rho_{0s}^i\right)\kappa, \tag{2.15}$$

$$\mathbf{u}^i\cdot\mathbf{n} = 0, \tag{2.16}$$

$$\rho_s^i \to \rho_{es}^i \quad \text{as } s_i \to \infty. \tag{2.17}$$

On the solid surface,

$$\gamma\alpha\frac{d}{ds}\left(\rho_s\frac{d\rho_s}{ds}\right) - \frac{1}{2}\frac{d}{ds}\left\{\rho_s(u_s+U)\right\} - \frac{\rho_s - \rho_{es}}{\tau} = 0, \tag{2.18}$$

$$\beta(u_s - U) = 2\mu\mathbf{n}\cdot\mathbf{e}\cdot(\mathbf{I}-\mathbf{nn}) - \frac{1}{2}\gamma\frac{d\rho_s}{ds}, \tag{2.19}$$

$$\mathbf{u}\cdot\mathbf{n} = 0, \tag{2.20}$$

$$\rho_s \to \rho_{es} \quad \text{as } s \to \infty, \tag{2.21}$$

where U is the speed of the contact line. At the contact line, $s = s_i = 0$, we have

$$-\rho_s^i\left\{u_s^i - \frac{\gamma\alpha(1+4A)}{4A}\frac{d\rho_s^i}{ds_i}\right\} = \rho_s\left\{\frac{1}{2}(u_s+U) - \gamma\alpha\frac{d\rho_s}{ds}\right\}, \tag{2.22}$$

and the force balance, (2.12). Equations (2.13) to (2.22) are all the equations for the unknown surface layer densities, ρ_s^i and ρ_s, and show how these quantities are coupled to the bulk velocities, shear stresses and normal stresses at the free and solid surfaces.

We can now see that we have steady nonlinear diffusion equations for the surface densities, (2.13) and (2.18), coupled to the flow through the forcing terms and the remaining equations[6]. These two second order equations require two boundary conditions at infinity, given by (2.17) and (2.21), and two conditions at the contact line, at first sight given by (2.12) and (2.22). However, the Young-Laplace equation, (2.12), determines the dynamic contact angle, θ_c, which is unknown *a priori*, and cannot therefore be counted as a connection condition for these two second order differential equations. Another condition is required at the contact line to close the system.

[5] Shikhmurzaev [24] suggests $A = 1/12$ as a plausible estimate for A based upon an analogy with channel flow.

[6] Note that, in an unsteady flow, $\partial\rho_s^i/\partial t$ and $\partial\rho_s/\partial t$ would appear on the right hand sides of (2.13) and (2.18) respectively.

https://doi.org/10.1017/S0956792506006589 Published online by Cambridge University Press

At this point, it is interesting to note the work presented in [20]. In this paper, the authors compute numerical solutions for a steady, two-dimensional plunging tape experiment, using a reduced version of Shikhmurzaev's theory. Their first approximation is to apply Shikhmurzaev's boundary conditions in a region close to the contact line only, which they refer to as the mesoscopic region. Outside this region (the macroscopic region), to increase computational efficiency, they use the standard boundary conditions of no slip on the solid surface and stress continuity and zero normal velocity on the free surface. Stress and flux continuity at the boundary between the mesoscopic and macroscopic regions then closes the problem. In essence, this is what we will be doing in §4 of this paper, except that, instead of attempting to simulate a particular problem in the macroscopic region ($s > s_\infty$ in §4), we assume that the flow is given by Moffat's solution for flow in a wedge with a free surface, (3.6), which we shall see is the appropriate outer solution for sufficiently small capillary number. In Monnier & Witomski [20], the authors, for the sake of simplicity, and to make code development easier, assume that the surface density on the free surface is constant. They state that they will return to the full problem in a later publication. With this assumption, they were able to solve the problem numerically, without applying an additional boundary condition at the contact line. Indeed, in this case they were able to prove that, for a given mass flux through the contact line, the nonlinear ordinary differential equation that governs the behaviour of the solid surface density, in the same form as (2.18), has a unique solution after making some reasonable assumptions about the behaviour of u_s. However, the fact that they obtain a unique solution when the surface density is artificially forced to be constant simply confirms the fact that when, instead, the second order differential equation (2.13) is solved on the free surface, an additional boundary condition is required at the contact line. The authors recognize this point, and are currently trying to show rigorously that an additional boundary condition is required (personal communication).

Shikhmurzaev derived the equations that govern the surface layer variables by considering the nonequilibrium thermodynamics of the surface, based upon the theory of Bedeaux, Albano and Mazur [3]. In particular, conservation of mass gives (2.3), whilst conservation of momentum gives that the normal component of the surface stress is zero, along with a generalized equation of capillarity. Conservation of energy can be used to derive the rate at which entropy is produced, which then leads to (2.5) and (2.7). Bedeaux has used this approach to consider the thermodynamics of the contact line [4]. The contact line can be treated as an independent thermodynamic entity, in the same manner as the surfaces. Then, making the reasonable assumption that there are no excess densities or fluxes along the contact line, three, not two, continuity conditions emerge from the analysis. Conservation of mass and momentum simply lead to mass flux continuity and the force balance at the contact line (2.11) and (2.12). By considering the rate at which entropy is produced at the contact line, the third condition emerges, and is given by

$$\rho_s(0)v_s(0) = k\left\{\mu_s^i(0) - \mu_s(0)\right\}, \tag{2.23}$$

where μ_s is the chemical potential and k is a constant. This says that the flow through the contact line is driven by a difference in the chemical potentials of the interfaces at the contact line. One assumption that underlies Shikhmurzaev's theory is that deviations from equilibrium are small enough that the chemical potential is linearly related to changes in

https://doi.org/10.1017/S0956792506006589 Published online by Cambridge University Press

surface density, so that

$$\mu_s = \mu_{es} + \left.\frac{d\mu_s}{d\rho_s}\right|_{\rho_s=\rho_{es}} (\rho_s - \rho_{es}).$$

In addition, since there is no flow through a static contact line, we must have $\mu_{es} = \mu^i_{es}$, and hence

$$\rho_s(0)v_s(0) = \rho_s(0)\left\{\frac{1}{2}(u_s + U) - \gamma\alpha\frac{d\rho_s}{ds}\right\} = U^i_0\left(\rho^i_s(0) - \rho^i_{es}\right) - U_0\left(\rho_s(0) - \rho_{es}\right), \quad (2.24)$$

where the material parameters U^i_0 and U_0 are

$$U^i_0 = k\left.\frac{d\mu^i_s}{d\rho^i_s}\right|_{\rho^i_s=\rho^i_{es}}, \quad U_0 = k\left.\frac{d\mu_s}{d\rho_s}\right|_{\rho_s=\rho_{es}}, \quad (2.25)$$

and have the dimensions of velocity. We would expect that an order of magnitude estimate of U_0 and U^i_0 is h/τ.

There are now two obvious questions concerning the results in Shikhmurzaev [24]. Firstly, how was it possible to find a unique solution for steady Stokes flow in a wedge at low capillary number when the system of governing equations was incomplete, and secondly, how does this new boundary condition affect the solution of the problem?

3 Asymptotic solution for steady Stokes flow in a wedge at low capillary number

As we have seen, Shikhmurzaev's theory leads to the coupling of the usual bulk fluid flow to a set of equations for surface layer quantities through the boundary conditions (2.2) to (2.10). Rather than tackle this daunting problem in its full generality, Shikhmurzaev made the sensible decision to start with a simple, but nontrivial, flow, namely steady Stokes flow with strong surface tension. Apart from the linearization of the Navier-Stokes equations, the main advantage of this is that the free surface is flat at leading order, so that the flow domain is a simple wedge. As we shall see, asymptotic methods can then be used to simplify the problem.

We work in terms of polar coordinates, (r, θ), with origin at the contact line and $\mathbf{u} = (u_r, u_\theta)$. If we define a stream function using

$$u_r = \frac{1}{r}\frac{\partial\psi}{\partial\theta}, \quad u_\theta = -\frac{\partial\psi}{\partial r}, \quad (3.1)$$

then in Stokes flow we need to solve the biharmonic equation

$$\nabla^4\psi = 0, \quad (3.2)$$

in the bulk fluid. To consider what happens in the far field, we need to think of the flow as being driven by some prescribed outer flow with the surface variables in equilibrium. As $r \to \infty$, we therefore use

$$\mathbf{u} \sim \mathbf{u}_\infty(r, \theta), \quad p \sim p_\infty(r, \theta). \quad (3.3)$$

We note that as $r \to \infty$, since $\rho_s \to \rho_{es}$ and, as we shall see below, the shear stress at the solid surface tends to zero as $s \to \infty$, we recover the usual boundary conditions of no slip

https://doi.org/10.1017/S0956792506006589 Published online by Cambridge University Press

at the solid surface and no tangential stress at the free surface in the far field. To find the far field stream function ψ_∞, we must therefore solve (3.2) subject to

$$\psi_\infty = 0, \quad \frac{\partial^2 \psi_\infty}{\partial \theta^2} = 0 \quad \text{at } \theta = \theta_\infty, \tag{3.4}$$

$$\psi_\infty = 0, \quad \frac{1}{r}\frac{\partial \psi_\infty}{\partial \theta} = 1 \quad \text{at } \theta = 0. \tag{3.5}$$

This gives

$$\psi_\infty \equiv r\frac{\{(\theta-\theta_\infty)\sin\theta - \theta\cos\theta_\infty \sin(\theta-\theta_\infty)\}}{\sin\theta_\infty\cos\theta_\infty - \theta_\infty} \equiv rf(\theta;\theta_\infty), \tag{3.6}$$

a streamfunction that was first written down by Moffatt [19]. We conclude that

$$\mathbf{u}_\infty = \left(\frac{df}{d\theta}(\theta;\theta_\infty), -f(\theta;\theta_\infty)\right), \quad p_\infty = -\frac{1}{r}\left\{\frac{d^3 f}{d\theta^3}(\theta;\theta_\infty) + \frac{df}{d\theta}(\theta;\theta_\infty)\right\}. \tag{3.7}$$

Note that it is this $O(1/r)$ singularity in the pressure, which leads to an $O(\log r)$ singularity in the force at the contact line, which in turn leads to the need for a modification of the no slip boundary condition in the neighbourhood of the contact line [12].

Before proceeding, we should note that there is a difficulty here, since the normal stress at, and hence the curvature of, the free surface is $O(1/r)$, which suggests that the slope grows like $\log r$ ar $r \to \infty$, instead of tending to the constant $\tan\theta_\infty$. Physically, viscous bending causes the free surface to deform slowly as $r \to \infty$. However, for $\mathrm{Ca} \ll 1$ the deformation of the free surface is small, provided that $\log r \ll \mathrm{Ca}^{-1}$ [12], a point that we shall return to later. We can therefore think of the far field flow given by ψ_∞ as being driven by the outer flow at some large distance $r = r_\infty$ away from the contact line.

3.1 Lengthscales and dimensionless variables

Tables 1 and 2 summarize the physical and dimensionless parameters that are used in the following analysis.

3.1.1 *The free surface*

At the free surface, we note that the shear rate, $\mathbf{n}\cdot\mathbf{e}\cdot(\mathbf{I}-\mathbf{nn})$, in (2.14) has dimensions of velocity over length. This means that an appropriate scale for the spatially-varying part of ρ_s is $\mu U/\gamma$, since we should scale velocities with the velocity of the solid surface, which drives the flow. We therefore define dimensionless variables

$$\rho_s^i = \rho_{es}^i + \frac{\mu U}{\gamma}\hat{\rho}_s^i, \quad \hat{u}_s^i = \frac{u_s^i}{U}, \quad \hat{\mathbf{e}} = \frac{L_i \mathbf{e}}{U}, \quad \hat{p} = \frac{L_i p}{\mu U}, \quad \hat{s}_i = \frac{s_i}{L_i}, \quad \hat{\kappa} = L_i\kappa,$$

where L_i is a lengthscale that we wish to determine. In terms of these variables, (2.13) becomes

$$\frac{\mu\alpha(1+4A)}{4AL_i}\frac{d}{d\hat{s}_i}\left\{\left(1+\frac{\mathrm{Ca}}{\lambda}\hat{\rho}_s^i\right)\frac{d\hat{\rho}_s^i}{d\hat{s}_i}\right\} - \frac{d}{d\hat{s}_i}\left\{\left(1+\frac{\mathrm{Ca}}{\lambda}\hat{\rho}_s^i\right)\hat{u}_s^i\right\} - \frac{\mu L_i}{\tau\gamma\rho_{es}^i}\hat{\rho}_s^i = 0, \tag{3.8}$$

https://doi.org/10.1017/S0956792506006589 Published online by Cambridge University Press

Table 1. *The physical parameters. Values are for water at room temperature*

Physical quantity	Symbol	Estimated typical value
surface layer thickness	h	10^{-10} m
surface layer compressibility	γ	2×10^6 m^{2}s^{-2}
surface layer relaxation timescale	τ	10^{-8} s
bulk fluid density	ρ	1000 kg m^{-3}
equilibrium surface layer density	ρ_{es}	$O(\rho h) \approx 10^{-7}$ kg m^{-2}
bulk fluid viscosity	μ	10^{-3} kg m^{-1} s^{-1}
coefficient of sliding friction	β	$O(\mu/h) \approx 10^7$ kg m^{-2} s^{-1}
a constant in equation (2.7)	α	$O(h/\mu) \approx 10^{-7}$ kg^{-1} m s
contact line speed	U	$\ll 70\,\mathrm{ms}^{-1}$
entropy production constants in (2.24)	U_0, U_0^i	$O(h/\tau) \approx 10^{-4}$ m s^{-1}
equilibrium surface tension	σ_e^i	7×10^{-2} N m^{-1}
Outer lengthscale	$L_{i1} = \tau\gamma\rho_{es}^i/\mu$	10^{-6} m
Inner lengthscale	$L_{i2} = \mu\alpha$	10^{-10} m
Slip lengthscale	$L = \sqrt{\alpha\gamma\rho_{es}^i\tau}$	10^{-8} m

Table 2. *The dimensionless parameters. Values are for water at room temperature*

Dimensionless parameter	Estimated typical value
$A = \alpha\beta$	1/12
$\mathrm{Ca} = \mu U/\sigma_e^i$	$\ll 1$
$\lambda = \gamma\rho_{es}^i/\sigma_e^i$	2.5
$K = \mu^2\alpha/\tau\gamma\rho_{es}^i$	10^{-4}
$\mathrm{Ca}_0 = \mu U_0/\sigma_e^i$	1.4×10^{-6}

where $\mathrm{Ca} = \mu U/\sigma_e^i \ll 1$ is the capillary number, σ_e^i is the equilibrium surface tension at the free surface and $\lambda = \gamma\rho_{es}^i/\sigma_e^i$. Using $\gamma \approx 2 \times 10^6\,\mathrm{m}^2\mathrm{s}^{-2}$, $\rho_{es}^i \approx 10^{-7}\,\mathrm{kg\,m}^{-2}$ and $\sigma_e^i \approx 0.07\,\mathrm{kg\,s}^{-2}$, we find that $\lambda \approx 2.5$. Since $\mathrm{Ca}/\lambda \ll 1$, (2.14) tells us that the driving velocity is small enough that the associated surface shear rate can produce only a small deviation of the surface density from its equilibrium value. Shikhmurzaev proceeds by assuming that $\lambda \gg 1$ [25], so that a small change in the surface density leads to a large change in the surface tension (an almost incompressible surface layer). In order to investigate how the analysis presented in Shikhmurzaev [25] leads to a unique solution, even though we have demonstrated that an additional boundary condition, (2.24), is required at the contact line, we will begin by assuming that $\lambda \gg 1$. Later in the paper, we will relax this assumption, and consider the solution when $\lambda = O(1)$.

We must now choose L_i to balance terms in (3.8). Balancing the second and third terms gives

$$L_i = L_{i1} \equiv \tau\gamma\rho_{es}^i/\mu.$$

Using the estimate $\tau \approx 10^{-5}\,\mu$ made by Blake & Shikhmurzaev [11], $L_{i1} \approx 10^{-6}$ m. Note, however, that we will revise this estimate later when we compare the model to the same experimental data set, but take into account the modified boundary condition (2.24) and

https://doi.org/10.1017/S0956792506006589 Published online by Cambridge University Press

the effect of viscous bending. With $L_i = L_{i1}$, (3.8) becomes

$$K\frac{1+4A}{4A}\frac{d}{d\hat{s}_i}\left\{\left(1+\frac{\mathrm{Ca}}{\lambda}\hat{\rho}_s^i\right)\frac{d\hat{\rho}_s^i}{d\hat{s}_i}\right\}-\frac{d}{d\hat{s}_i}\left\{\left(1+\frac{\mathrm{Ca}}{\lambda}\hat{\rho}_s^i\right)\hat{u}_s^i\right\}-\hat{\rho}_s^i=0, \tag{3.9}$$

where $K=\mu^2\alpha/\tau\gamma\rho_{es}^i\approx 10^{-4}\ll 1$, using the estimate $\alpha=h/\mu$. Recall that $h\approx 10^{-10}$ m is an estimate of the thickness of the surface layer. Since $K\ll 1$, we expect that the solution on this lengthscale will be an outer solution, and that the second derivative term will come into play on a smaller, inner lengthscale. We also have

$$2\mathbf{n}\cdot\hat{\mathbf{e}}\cdot(\mathbf{I}-\mathbf{nn})=\frac{d\hat{\rho}_s^i}{d\hat{s}_i}, \tag{3.10}$$

$$\mathrm{Ca}\,(-\hat{p}+2\mathbf{n}\cdot\hat{\mathbf{e}}\cdot\mathbf{n})=-\left(1-\mathrm{Ca}\hat{\rho}_s^i\right)\hat{\kappa}, \tag{3.11}$$

$$\hat{\rho}_s^i\to 0\quad\text{as }\hat{s}_i\to\infty. \tag{3.12}$$

Note that, since $\mathrm{Ca}\ll 1$, we have $\hat{\kappa}\ll 1$, so that, at leading order, the free surface is a straight line, with $\theta_\infty=\theta_c$. This remains true for all of the scalings that we consider in this section, and, at leading order, the domain of solution is therefore the wedge $0<\theta<\theta_c$, and we need not consider the normal stress balance further. Note that θ_c remains to be determined. Since the free surface is flat at leading order, we can now write $r=s=s_i$.

Returning to consider (3.8), we cannot balance the first and third terms on a lengthscale smaller than L_{i1}, but by taking $L_i=L_{i2}\equiv KL_{i1}=\mu\alpha$, we obtain

$$\frac{1+4A}{4A}\frac{d}{d\bar{r}}\left\{\left(1+\frac{\mathrm{Ca}}{\lambda}\hat{\rho}_s^i\right)\frac{d\hat{\rho}_s^i}{d\bar{r}}\right\}-\frac{d}{d\bar{r}}\left\{\left(1+\frac{\mathrm{Ca}}{\lambda}\hat{\rho}_s^i\right)\hat{u}_s^i\right\}-K\hat{\rho}_s^i=0, \tag{3.13}$$

$$2\mathbf{n}\cdot\hat{\mathbf{e}}\cdot(\mathbf{I}-\mathbf{nn})=\frac{d\hat{\rho}_s^i}{d\bar{r}}, \tag{3.14}$$

where $\bar{r}=r/L_{i2}$. We will also see below that it is the flow in the solid surface layer that drives the bulk flow and the flow in the free surface layer, so that the details of the flow in this inner region are not important, at least when $\mathrm{Ca}\ll 1$. Therefore, although our order of magnitude estimate for L_{i2} is h, so that this lengthscale is roughly that of the surface layer, and hence the continuum approximation starts to break down, we should not be unduly concerned.

3.1.2 *The solid surface*

On the solid surface, (2.19) does not suggest any restriction on changes in ρ_s. This means that there is only one possible choice of lengthscale, $L\equiv\sqrt{\alpha\gamma\rho_{es}^i\tau}=K^{1/2}L_{i1}=K^{-1/2}L_{i2}\approx 10^{-8}$ m. We refer to this as the slip region. We define dimensionless variables

$$\tilde{\rho}_s=\frac{\rho_s}{\rho_{es}^i},\quad \tilde{u}_s=\frac{u_s}{U},\quad \tilde{r}=\frac{r}{L},$$

in terms of which (2.18) and (2.19) become

$$\frac{d}{d\tilde{r}}\left(\tilde{\rho}_s\frac{d\tilde{\rho}_s}{d\tilde{r}}\right)-\frac{\mathrm{Ca}}{2\lambda K^{1/2}}\frac{d}{d\tilde{r}}\left\{\tilde{\rho}_s\left(\tilde{u}_s+1\right)\right\}-\left(\tilde{\rho}_s-\tilde{\rho}_{es}\right)=0, \tag{3.15}$$

$$A\mathrm{Ca}\left(\tilde{u}_s-1\right)=K^{1/2}\left\{2\mathrm{Ca}\,\mathbf{n}\cdot\tilde{\mathbf{e}}\cdot(\mathbf{I}-\mathbf{nn})-\frac{1}{2}\lambda\frac{d\tilde{\rho}_s}{d\tilde{r}}\right\}, \tag{3.16}$$

where $\tilde{\rho}_{es}=\rho_{es}/\rho_{es}^i$.

https://doi.org/10.1017/S0956792506006589 Published online by Cambridge University Press

Note that L_{i1}, L_{i2} and L are material parameters, independent of U. It is interesting that $U\tau$, the obvious lengthscale on the solid surface based on fluid particles taking a time τ to relax to their equilibrium state after passing through the contact line at speed U, does not emerge from this analysis, since, when Ca is sufficiently small, the relaxation of the surface density to its equilibrium value is governed by the first and third terms of (3.15). The second, advective term is small. In fact, $U\tau/L = \mathrm{Ca}/\lambda K^{1/2}$, so that advection by the solid surface becomes important when $\mathrm{Ca} = O(\lambda K^{1/2})$.

3.1.3 *The contact line*

At the contact line, we have

$$\cos\theta_c - \cos\theta_s = \lambda(\tilde{\rho}_{es} - \tilde{\rho}_s) - \mathrm{Ca}\cos\theta_c\hat{\rho}_s^i, \tag{3.17}$$

$$-\left(1 + \frac{\mathrm{Ca}}{\lambda}\hat{\rho}_s^i\right)\left(\hat{u}_s^i - \frac{1+4A}{4A}\frac{d\hat{\rho}_s^i}{d\hat{r}}\right) = \tilde{\rho}_s\left\{\frac{1}{2}(\tilde{u}_s+1) - \frac{\lambda K^{1/2}}{\mathrm{Ca}}\frac{d\tilde{\rho}_s}{d\tilde{r}}\right\}$$
$$= \frac{\mathrm{Ca}_0^i}{\lambda}\hat{\rho}_s^i - \frac{\mathrm{Ca}_0}{\mathrm{Ca}}(\tilde{\rho}_s - \tilde{\rho}_{es}), \tag{3.18}$$

where

$$\mathrm{Ca}_0^i = \frac{\mu U_0^i}{\sigma_e^i}, \quad \mathrm{Ca}_0 = \frac{\mu U_0}{\sigma_e^i}.$$

Using the estimate $U_0^i \approx U_0 \approx h/\tau$, we find that $\mathrm{Ca}_0^i \approx \mathrm{Ca}_0 \approx 10^{-4}$. Now the force balance, (3.17), shows that for $-1 \leqslant \cos\theta_c \leqslant 1$ we need $\tilde{\rho}_{es} - \tilde{\rho}_s = O(\lambda^{-1})$ when $\lambda \gg 1$. We therefore define

$$\tilde{\rho}_s = \tilde{\rho}_{es} + \frac{\bar{\rho}_s}{\lambda}, \tag{3.19}$$

so that

$$\cos\theta_c - \cos\theta_s = \bar{\rho}_s - \mathrm{Ca}\cos\theta_c\hat{\rho}_s^i, \tag{3.20}$$

$$-\left(1 + \frac{\mathrm{Ca}}{\lambda}\hat{\rho}_s^i\right)\left(\hat{u}_s^i - \frac{1+4A}{4A}\frac{d\hat{\rho}_s^i}{d\hat{r}}\right) = \left(\tilde{\rho}_{es} + \frac{\bar{\rho}_s}{\lambda}\right)\left\{\frac{1}{2}(\tilde{u}_s+1) - \frac{K^{1/2}}{\mathrm{Ca}}\frac{d\bar{\rho}_s}{d\tilde{r}}\right\}$$
$$= \frac{\mathrm{Ca}_0^i}{\lambda}\hat{\rho}_s^i - \frac{\mathrm{Ca}_0}{\lambda\mathrm{Ca}}\bar{\rho}_s, \tag{3.21}$$

and (3.15) and (3.16) become

$$\frac{d}{d\tilde{r}}\left\{\left(\tilde{\rho}_{es} + \frac{\bar{\rho}_s}{\lambda}\right)\frac{d\bar{\rho}_s}{d\tilde{r}}\right\} - \frac{\mathrm{Ca}}{2K^{1/2}}\frac{d}{d\tilde{r}}\left\{\left(\tilde{\rho}_{es} + \frac{\bar{\rho}_s}{\lambda}\right)(\tilde{u}_s+1)\right\} - \bar{\rho}_s = 0, \tag{3.22}$$

$$A\mathrm{Ca}(\tilde{u}_s - 1) = K^{1/2}\left\{2\mathrm{Ca}\,\mathbf{n}\cdot\tilde{\mathbf{e}}\cdot(\mathbf{I} - \mathbf{nn}) - \frac{1}{2}\frac{d\bar{\rho}_s}{d\tilde{r}}\right\}. \tag{3.23}$$

https://doi.org/10.1017/S0956792506006589 Published online by Cambridge University Press

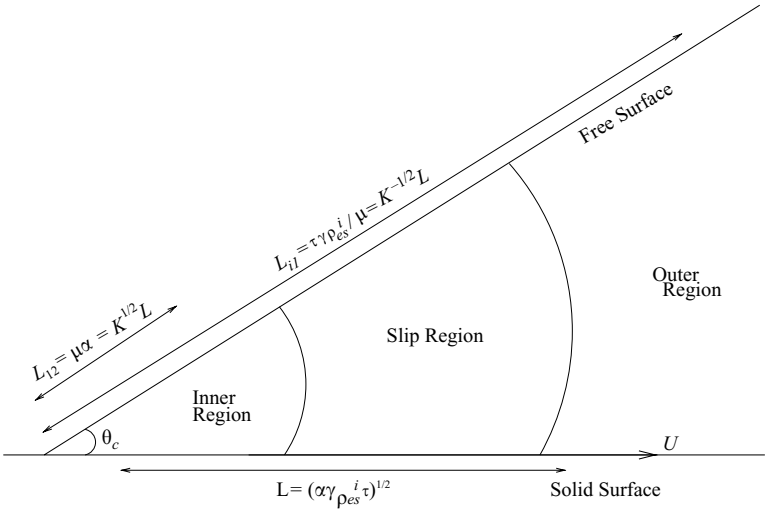


FIGURE 2. The three asymptotic regions and their lengthscales.

3.2 Solution in the three asymptotic regions

We can now pull all of this together and consider the leading order solutions in the inner, outer and slip regions, which are illustrated in Figure 2. We assume that $\lambda \gg 1$, $K \ll 1$, $\mathrm{Ca} \ll 1$ with $\lambda K^{1/2} = O(1)$ and $\lambda \mathrm{Ca} = O(1)$, since this is a distinguished limit. Note that for $\lambda \gg 1$, $\tilde{\rho}_{es} = 1 + O(\lambda^{-1})$. Our aim is to solve the boundary value problem, and determine how the dynamic contact angle, θ_c, varies as a function of the capillary number, Ca, and hence with the contact line velocity, U, for fixed values of the other parameters. Although we have given order of magnitude estimates of the other parameters, there remains considerable uncertainty as to there sizes.

3.2.1 *Slip region : $r = O(L)$*

In this region, at leading order, neglecting terms of $O(\mathrm{Ca})$, (3.22) and (3.23) become

$$\frac{d^2\bar{\rho}_s}{d\tilde{r}^2} - \frac{\mathrm{Ca}}{2K^{1/2}}\frac{d\tilde{u}_s}{d\tilde{r}} - \bar{\rho}_s = 0, \tag{3.24}$$

$$\tilde{u}_s = 1 - \frac{K^{1/2}}{2A\mathrm{Ca}}\frac{d\bar{\rho}_s}{d\tilde{r}}, \tag{3.25}$$

and hence

$$\frac{1+4A}{4A}\frac{d^2\bar{\rho}_s}{d\tilde{r}^2} - \bar{\rho}_s = 0. \tag{3.26}$$

The solution that satisfies $\bar{\rho}_s \to 0$ as $\tilde{r} \to \infty$ is

$$\bar{\rho}_s = \bar{\rho}_s(0)\exp\left(-\sqrt{\frac{4A}{1+4A}}\tilde{r}\right). \tag{3.27}$$

https://doi.org/10.1017/S0956792506006589 Published online by Cambridge University Press

Equations (3.18) and (3.20) give

$$\cos\theta_c - \cos\theta_s = \bar{\rho}_s(0), \tag{3.28}$$

$$\frac{1}{2}(\tilde{u}_s(0)+1) - \frac{K^{1/2}}{\mathrm{Ca}}\frac{d\bar{\rho}_s}{d\tilde{r}}(0) = -\frac{\mathrm{Ca}_0}{\lambda \mathrm{Ca}}\bar{\rho}_s, \tag{3.29}$$

assuming that Ca_0 and Ca_0^i are of $O(1)$. Using the solution (3.27), we find that

$$\cos\theta_c - \cos\theta_s = \bar{\rho}_s(0) = -\frac{U}{U_c}, \tag{3.30}$$

where

$$U_c = \frac{1}{\lambda}\left\{U_0 + \sqrt{\frac{\gamma\alpha\rho_{es}^i(1+4A)}{4A\tau}}\right\}. \tag{3.31}$$

Equation (3.30) says that the theory predicts a linear variation of the cosine of the actual contact angle with contact line velocity. Since this is not in good agreement with experimental observations of the dynamic contact angle, we will consider the solution when $\lambda = O(1)$ and $\mathrm{Ca} = O(1)$ in §4. It is also interesting to note that a result of the same form as (3.30) was derived in Linder-Silwester & Schneider [17], which addresses the small capillary number, large Reynolds number limit of this problem[7].

Note that we have been able to determine the surface density distribution on the solid surface without having to solve on either the free surface or in the bulk. We can see that the solid surface drives the bulk flow through the boundary condition

$$\tilde{u}_s = 1 - \frac{1}{\mathrm{Ca}_c}\sqrt{\frac{K}{A(1+4A)}}\exp\left(-\sqrt{\frac{4A}{1+4A}}\tilde{r}\right), \tag{3.32}$$

where $\mathrm{Ca}_c = \mu U_c/\sigma_e$. As we shall see below, this also drives the behaviour of the free surface density.

3.2.2 *Outer region: $r = O(L_{i1})$*

At leading order, neglecting terms of $O(\mathrm{Ca})$, the solid surface variables take their equilibrium values, with $\tilde{\rho}_s = 1$, $\tilde{u}_\theta = 0$ and $\tilde{u}_s = \tilde{u}_r = 1$ at $\theta = 0$. On the free surface, (3.9) and (3.10) become, at leading order

$$\frac{d\hat{u}_r}{d\hat{r}} = -\hat{\rho}_s^i, \tag{3.33}$$

$$\frac{d\hat{\rho}_s^i}{d\hat{r}} = -\frac{1}{\hat{r}}\frac{\partial\hat{u}_r}{\partial\theta}. \tag{3.34}$$

If we eliminate $\hat{\rho}_s^i$ between these equations, we arrive at the boundary value problem

$$\nabla^4\psi = 0 \quad \text{for } \hat{r} > 0,\ 0 < \theta < \theta_c, \tag{3.35}$$

[7] Although the authors discuss the asymptotic structure of the solution, no equations are actually solved in Linder-Silwester & Schneider [17], apart from the equation for the surface density at the solid surface, so the issue of the number of boundary conditions required did not arise.

https://doi.org/10.1017/S0956792506006589 Published online by Cambridge University Press

to be solved subject to

$$\psi = 0, \quad \frac{1}{\hat{r}}\frac{\partial \psi}{\partial \theta} = 1 \quad \text{at } \theta = 0, \tag{3.36}$$

$$\psi = 0, \quad \frac{d^2}{d\hat{r}^2}\left\{\frac{1}{\hat{r}}\frac{\partial \psi}{\partial \theta}\right\} = \frac{1}{\hat{r}^2}\frac{\partial^2 \psi}{\partial \theta^2} \quad \text{at } \theta = \theta_c, \tag{3.37}$$

$$\psi \sim \psi_\infty \quad \text{as } \hat{r} \to \infty. \tag{3.38}$$

Of course, one solution of this boundary value problem is $\psi = \psi_\infty$, given by (3.6). In other words, there is a solution available where the far field is attained with $\hat{r} = o(1)$, and effectively this asymptotic region is not needed. This is the solution used in Shikhmurzaev [24]. However, we will now show that this solution is *not* unique. It is easy to miss this possibility, and the present author made the same mistake in an earlier publication [5].

We begin by defining

$$\psi = \psi_\infty + \Psi.$$

Because the far field stream function, ψ_∞, is a solution of the boundary value problem given by (3.35) to (3.38), in particular, since it corresponds to a constant velocity and no shear stress at the free surface, we arrive at the boundary value problem

$$\nabla^4 \Psi = 0, \tag{3.39}$$

subject to

$$\Psi = 0, \quad \frac{\partial \Psi}{\partial \theta} = 0 \quad \text{at } \theta = 0, \tag{3.40}$$

$$\Psi = 0, \quad \frac{d^2}{d\hat{r}^2}\left\{\frac{1}{\hat{r}}\frac{\partial \Psi}{\partial \theta}\right\} = \frac{1}{\hat{r}^2}\frac{\partial^2 \Psi}{\partial \theta^2} \quad \text{at } \theta = \theta_c, \tag{3.41}$$

$$\Psi \to 0 \quad \text{as } \hat{r} \to \infty. \tag{3.42}$$

The homogeneous boundary value problem given by (3.39) to (3.42) has a nonzero solution for each value of θ_c with $0 < \theta_c < \pi$. Details are given in appendix A, where we find the solution analytically using Mellin integral transforms.

The solution we have constructed in this region will become nonuniform as $\hat{r} \to 0$ and we enter the inner region. As $\hat{r} \to 0$, we find that[8]

$$\psi \sim \hat{r} f(\theta; \theta_c) - \hat{r} u_\infty \frac{\theta_c \sin \theta_c}{\sin^2 \theta_c - \theta_c^2}\left\{\left(1 - \frac{\theta}{\theta_c}\right)\sin\theta + \frac{\theta \sin(\theta - \theta_c)}{\sin \theta_c}\right\}, \tag{3.43}$$

$$u_r|_{\theta=\theta_c} \to u_0(\theta_c) + u_\infty, \tag{3.44}$$

[8] The leading order small $\hat{r}$ asymptotic solution, (3.43), does not satisfy $(3.41)_2$ by itself, since $(3.41)_2$ is not homogeneous in $\hat{r}$, and therefore couples the $O(\hat{r})$ and $O(\hat{r}^2 \log \hat{r})$ terms in the expansion. The asymptotic expansion (3.43) can be deduced from the residue at the pole at $s = -1$ of the Mellin transform of the solution (see Appendix A).

https://doi.org/10.1017/S0956792506006589 Published online by Cambridge University Press

where f is Moffatt's solution, given by (3.6), u_0 is the tangential velocity on the free surface in Moffatt's solution, given by

$$u_0(\theta_c) = \frac{\sin\theta_c - \theta_c\cos\theta_c}{\sin\theta_c\cos\theta_c - \theta_c},$$

which is the free surface velocity in the far field, and u_∞ is an undetermined parameter that multiplies the solution of the homogeneous boundary value problem.

3.2.3 *Inner region : $r = O(L_{i2})$*

In this region, the bulk velocity is able to tend to zero at the contact line, so that there is no stress singularity there. The leading order versions of (3.10) and (3.13), neglecting terms of $O(\mathrm{Ca})$, show that

$$\frac{1}{\bar r}\frac{\partial \hat u_r}{\partial\theta} = -\frac{\partial\hat\rho_s^i}{\partial\bar r} = \frac{4A}{1+4A}\left\{\hat u_r - u_\infty - u_0(\theta_c)\right\}, \quad \hat u_\theta = 0 \ \text{ at } \theta = \theta_c. \tag{3.45}$$

On the solid surface, making use of the solution (3.27), we find that

$$\bar u_r - 1 = \frac{2}{A\bar r}\frac{\partial\bar u_r}{\partial\theta} - \frac{K^{1/2}}{\mathrm{Ca}_c}\frac{1}{\sqrt{A(1+4A)}} \ \text{ at } \theta = 0. \tag{3.46}$$

The boundary conditions (3.45) and (3.46), which take the form of Navier slip conditions, allow the radial velocities at the two bounding surfaces to undergo apparent slip, and thereby avoid a singularity in the force at the contact line. Once the solution of the bulk problem is known, we can, in principle, solve (3.45) for $\hat\rho_s^i$, making use of the boundary conditions (3.21) at $\bar r = 0$. This determines the constant u_∞, which appears in the solution in the outer region. In other words, the strength of the flow given by the solution of the homogeneous boundary value problem in the outer region is determined by conservation of mass at the contact line. In the original analysis, [24], [26], the boundary condition $(3.21)_2$ at the contact line was effectively replaced by the condition $u_\infty = 0$. There is no obvious way of selecting the asymptotic solution with $u_\infty = 0$ by imposing a boundary condition at the contact line.

4 Numerical solutions for $\mathrm{Ca} = O(1)$

Since we have chosen the dimensionless parameters so that the contact line speed, U, only appears in the capillary number, we can consider the effect of viscous bending at sufficiently high contact line speeds by taking $\mathrm{Ca} = O(1)$, but with λ still large and $\lambda K^{1/2} = O(1)$. We find that, on both surfaces, as above for $\mathrm{Ca} \ll 1$, the surface density is an $O(\lambda^{-1})$ correction to its equilibrium value. This means that the surface problems can be linearized. However, the solid surface density is now coupled to both the bulk flow and the flow on the free surface. Moreover, the normal stress balance on the free surface now gives an $O(1)$ deformation, so we are faced with a nonlinear free boundary problem, even though all the other equations can be linearized. For these reasons, and also because we would like to investigate what happens when $\lambda = O(1)$, we will solve the full nonlinear problem numerically, treating all parameters as $O(1)$.

https://doi.org/10.1017/S0956792506006589 Published online by Cambridge University Press

We will use the slip lengthscale $L = \sqrt{\alpha\gamma\rho_{es}^i\tau}$ to nondimensionalise the equations. In addition, since it is convenient to be able to set $\mathrm{Ca} = 0$ and obtain the static solution, we will not nondimensionalise velocities and stresses using the contact line speed U, but use σ_e^i/μ instead. The full dimensionless problem is then

$$\nabla\cdot\mathbf{u} = 0, \quad 0 = -\nabla p + \nabla^2\mathbf{u} \ \text{ in } D, \tag{4.1}$$

where D is the region occupied by the bulk fluid,

$$\frac{d}{dr}\left(\rho_s\frac{d\rho_s}{dr}\right) - \frac{1}{2\lambda K^{1/2}}\frac{d}{dr}\left\{\rho_s\left(u_s + \mathrm{Ca}\right)\right\} - \left(\rho_s - \tilde{\rho}_{es}\right) = 0 \ \text{ on } \partial D_1, \tag{4.2}$$

$$A\left(u_s - \mathrm{Ca}\right) = 2K^{1/2}\,\mathbf{f}_1\cdot(\mathbf{I}-\mathbf{nn}) - \frac{1}{2}\lambda K^{1/2}\frac{d\rho_s}{dr} \ \text{ on } \partial D_1, \tag{4.3}$$

where ∂D_1 is the solid surface and $\mathbf{f}_1$ the force exerted on the solid surface by the fluid,

$$\frac{1+4A}{4A}\frac{d}{ds}\left(\rho_s^i\frac{d\rho_s^i}{ds}\right) - \frac{1}{\lambda K^{1/2}}\frac{d}{ds}\left(\rho_s^i u_s^i\right) - \left(\rho_s^i - 1\right) = 0 \ \text{ on } \partial D_2, \tag{4.4}$$

$$\mathbf{f}_2\cdot(\mathbf{I}-\mathbf{nn}) = \lambda\frac{d\rho_s^i}{ds} \ \text{ on } \partial D_2, \tag{4.5}$$

$$\mathbf{f}_2\cdot\mathbf{n} = \left(\lambda + 1 - \lambda\rho_s^i\right)\kappa \ \text{ on } \partial D_2, \tag{4.6}$$

where ∂D_2 is the free surface and $\mathbf{f}_2$ the force exerted on the free surface by the fluid. At the contact line, $s = r = 0$,

$$\cos\theta_c = \frac{\cos\theta_s - \lambda\left(\tilde{\rho}_{es} - \rho_s(0)\right)}{1 - \lambda\left(\rho_s^i(0) - 1\right)}, \tag{4.7}$$

$$\begin{aligned} -\rho_s^i\left\{u_s^i - \frac{1+4A}{4A}\lambda K^{1/2}\frac{d\rho_s^i}{ds}\right\} &= \rho_s\left\{\frac{1}{2}\left(u_s + \mathrm{Ca}\right) - \lambda K^{1/2}\frac{d\rho_s}{dr}\right\} \\ &= \mathrm{Ca}_0^i\left(\rho_s^i - 1\right) - \mathrm{Ca}_0\left(\rho_s - \tilde{\rho}_{es}\right). \end{aligned} \tag{4.8}$$

We treat the far field conditions by assuming that the flow a distance s_∞ away from the contact line along the free surface takes the form given by (3.6) and (3.7). Of course, this is only appropriate for sufficiently small values of Ca, but it allows us to capture the effect of viscous bending, which leads to a slow but significant increase in the slope of the free surface as s_i increases. The approach used in [20], which we discussed earlier, with a macroscopic region for $r > r_\infty$ where the ordinary boundary conditions are applied, would be more appropriate for larger values of Ca.

The Stokes equations, (4.1), can be rewritten in boundary integral form as

$$\mathbf{u}(\mathbf{x}_0) = \frac{1}{2\pi}\int_B\left\{-\mathbf{f}(\mathbf{x})\log\hat{r} + \frac{\hat{\mathbf{x}}\left(\mathbf{f}\cdot\hat{\mathbf{x}}\right)}{\hat{r}^2} + \frac{4\left(\mathbf{u}(\mathbf{x})\cdot\hat{\mathbf{x}}\right)\left(\mathbf{n}(\mathbf{x})\cdot\hat{\mathbf{x}}\right)\hat{\mathbf{x}}}{\hat{r}^4}\right\}ds(\mathbf{x}), \tag{4.9}$$

where B is the boundary of the domain of solution, $\mathbf{x}_0$ is a point on B, but not a corner point, $\hat{\mathbf{x}} = \mathbf{x} - \mathbf{x}_0$ and $\hat{r} = |\hat{\mathbf{x}}|$ [22]. This is an extremely convienient way of treating this

https://doi.org/10.1017/S0956792506006589 Published online by Cambridge University Press

problem, since the boundary conditions can all be written in terms of **f** and **u**. We truncate the infinite domain using the arc of a circle, and assume that **f** and **u** are given there by the far field solution (3.6) and (3.7).

We discretize the free and solid surfaces at N points, using a nonuniform grid spacing in order to capture the three natural lengthscales of the problem ($O(K^{1/2})$, $O(1)$ and $O(K^{-1/2})$), typically with $N = 500$. On every boundary element we assume that each of ρ_s, u_s and **f** is constant. Since we know that the normal component of the fluid velocity is zero at each surface, there are four unknowns on each element. We discretize the derivatives in the boundary conditions using finite differences, and evaluate the boundary integral equation (4.9) using two point Gaussian quadrature, collocating at the midpoint of each linear element. We solve the problem in an iterative manner. Starting from an initial guess of the position of the free surface, we solve the discrete version of the boundary value problem without (4.6) and (4.7), using Newton's method. We then obtain an updated position of the free surface by solving (4.6), using (4.7) as the initial condition. We repeat these two procedures until the position of the free surface has converged.

4.1 A typical solution

We begin by showing that our numerical solutions are in agreement with the asymptotic solution that we developed in the previous section. We take $K = 10^{-4}$ and $\lambda = 100$, so that $\lambda K^{1/2} = 1$, and use $\theta_s = 60^\circ$ as a convenient value for the static contact angle. We then take all of the other parameters to be unity: $A = \tilde{\rho}_{es} = \mathrm{Ca}_0^i = \mathrm{Ca}_0 = 1$. In this, and the other numerical solutions that we present, we take $s_\infty = 25K^{-1/2}$ to ensure that the solution in the outer asymptotic region has converged.

Figure 3 shows the variation of the contact angle with Ca. We have plotted θ_c, the microscopic dynamic contact angle at the point where the free surface meets the solid surface, θ_{app}, the angle that the free surface makes with the x-axis at $s = s_{app}$, a point at which we assume accurate experimental measurement is possible, and θ_{as}, the microscopic dynamic contact angle given by the asymptotic solution (3.30). If the slip lengthscale is approximately 10^{-8}m, as discussed above, and we assume that accurate experimental measurement of the angle of the free surface can be made 10^{-5} m from the contact line, this suggests that it is reasonable to take $s_{app} = 1000$. We can see that the asymptotic prediction of θ_c is almost indistinguishable from the numerical solution, and, from the small difference between θ_c and θ_{app}, that there is a little viscous bending. Also shown is θ_{cox}, the value of the apparent contact angle predicted by the asymptotic solution derived by Cox, [12], assuming a slip length firstly 10^3 and secondly 10^5 times smaller than the lengthscale upon which the apparent contact angle is measured ($s = 1$ and $s = 10^{-2}$), with the microscopic contact angle given by θ_c. It is clear that the asymptotic solution with a slip length 10^5 times smaller than the lengthscale of the measurement of θ_{app} is in the better agreement with the numerical solution. This leads us to point out that the lengthscale over which the singularity in the shear stress is relieved is the inner length scale of $O(K^{1/2}) \ll 1$, *not* the $O(1)$ slip lengthscale. Although there is slip between the solid surface and the fluid on the slip lengthscale due to the surface tension gradient, the bulk fluid velocity does not tend to zero on this lengthscale, and hence there is still significant viscous bending. It is only in the inner region that slip is driven by the

https://doi.org/10.1017/S0956792506006589 Published online by Cambridge University Press

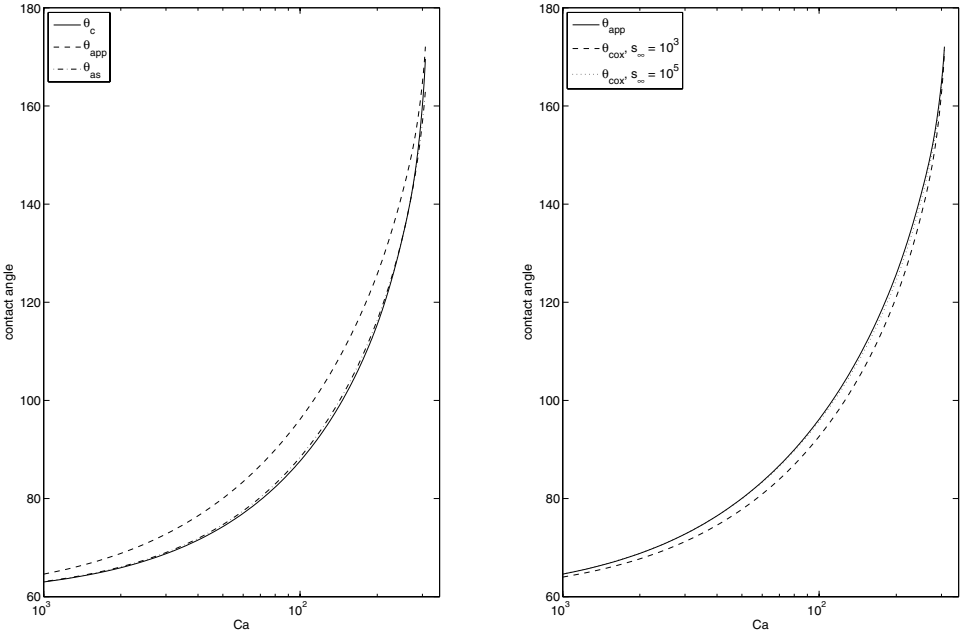


FIGURE 3. The actual contact angle, θ_c, apparent contact angle, θ_{app}, asymptotic prediction of the actual contact angle, θ_{as}, and the apparent contact angle, θ_{cox}, predicted by Cox's analysis for two different slip lengths for the typical case described in §4.1.

shear stress, and the fluid velocities tend to zero, relieving the apparent stress singularity and associated viscous bending [12]. In Shikhmurzaev [24] and subsequent papers, it is assumed that viscous bending stops in the slip region, not the inner region, which means that the amount of viscous bending is underestimated. We shall return to this point later.

In order to give us more confidence in our numerical solutions, we also calculated the deformation of the free surface with Shikhmurzaev's boundary conditions replaced by no shear on the free surface and Navier slip on a dimensionless lengthscale of unity. This is a simpler problem, to which Cox's analysis is also applicable. Figure 4 shows the behaviour of the apparent contact angle when the actual contact angle is fixed at $\theta_c = 60^\circ$. We were able to calculate the position of the free surface up to Ca ≈ 0.5 before our iterative procedure failed to converge. There is excellent agreement between the numerical solution and Cox's asymptotic solution, even when Ca is not very small. Note also that viscous bending is certainly not negligible for capillary numbers greater than about 0.01.

Figures 5 and 6 show the variations of the surface densities and velocities when Ca $= 10^{-3}$. The change in the free surface density is much smaller than that in the solid surface density, as predicted by the asymptotic theory. It is also clear that the free surface density varies over a much longer lengthscale than the solid surface density, of $O(K^{-1/2}) \approx 10^2$, as predicted again by the asymptotic theory. Also shown is the asymptotic solution for the solid surface density. As we would expect, there is good agreement over $O(1)$ lengthscales, but some variation on the shorter, inner lengthscale, $s = O(K^{1/2}) \approx 10^{-2}$. The solid surface layer velocity, shown in figure 6, similarly is in good agreement over $O(1)$

https://doi.org/10.1017/S0956792506006589 Published online by Cambridge University Press

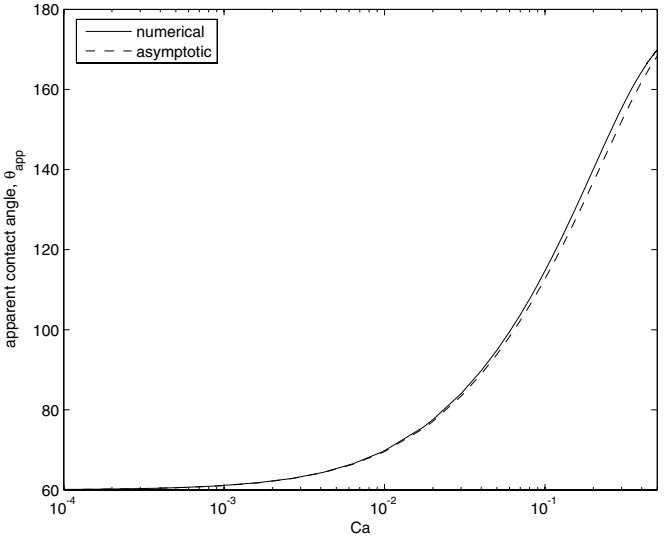


FIGURE 4. The apparent contact angle measured at $s = s_{app} = 1000$, with $\theta_c = \theta_s = 60^o$ and Navier slip, calculated both numerically and using Cox's asymptotic analysis.

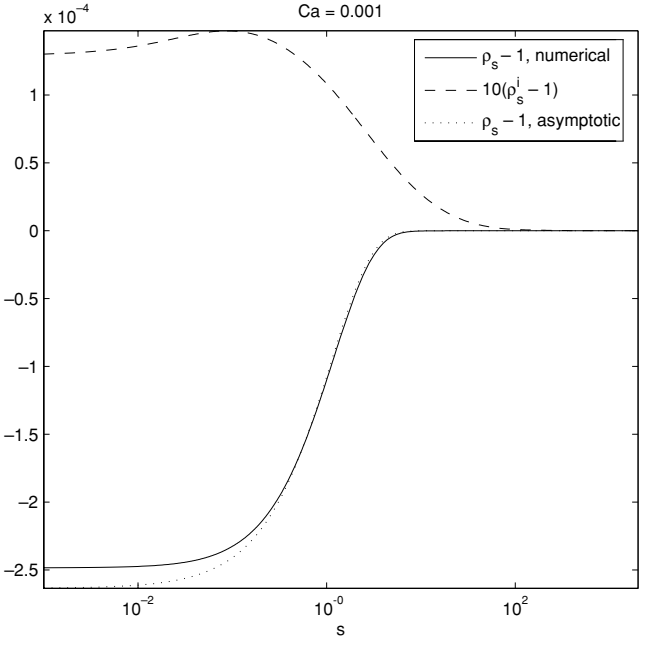


FIGURE 5. The surface densities when Ca = 0.001 for the typical case described in section 4.1. Also shown is the asymptotic solution on the solid surface. The change in the free surface density, $\rho_s^i - 1$, is scaled by a factor of ten so that its qualitative form can be seen clearly.

https://doi.org/10.1017/S0956792506006589 Published online by Cambridge University Press

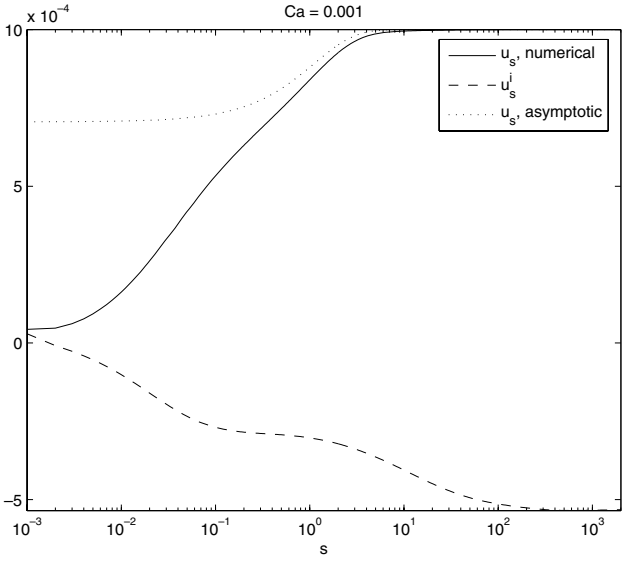


FIGURE 6. The surface velocities when Ca = 0.001 for the typical case described in § 4.1.

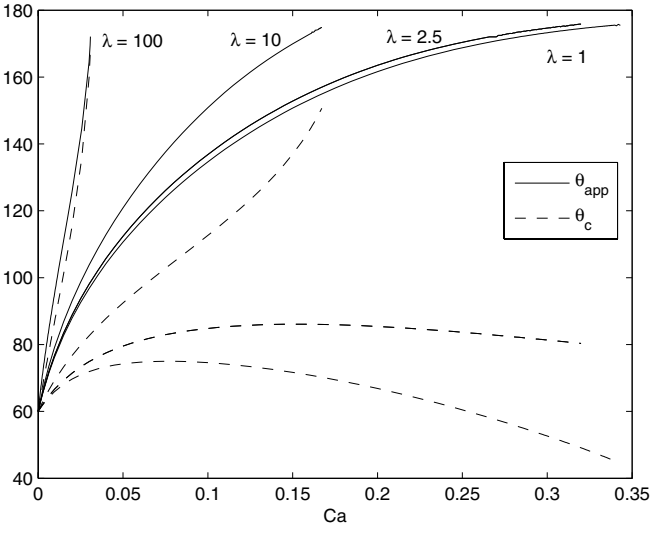


FIGURE 7. The microscopic and apparent contact angles, plotted for various values of λ. In each case, the apparent contact angle is larger than the microscopic contact angle.

lengthscales, but then changes significantly over the inner lengthscale. The free surface layer velocity clearly shows the type of behaviour predicted by the small Ca asymptotic solution. Over an $O(1)$ lengthscale, the velocity is almost constant at around -3×10^{-4}, but then asymptotes to the far field velocity over the longer, outer lengthscale.

By varying the parameters in the problem, we find that the solution is most sensitive to changes in λ, which characterizes the compressibility of the surface layers. Figure 7

https://doi.org/10.1017/S0956792506006589 Published online by Cambridge University Press

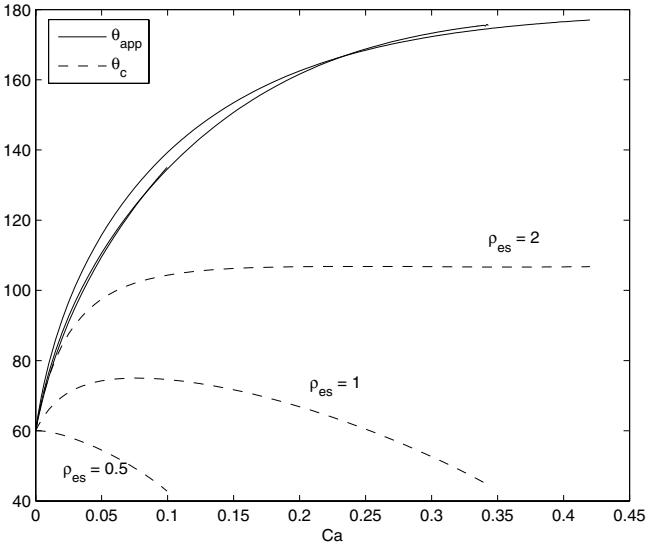


FIGURE 8. The microscopic and apparent contact angles, plotted for various values of $\tilde{\rho}_{es}$. In each case, the apparent contact angle is larger than the microscopic contact angle.

shows how the actual and apparent contact angles change as λ decreases. We can see that these contact angles remain below 180° for a greater range of values of Ca the lower λ becomes, and that, for sufficiently low values of λ, the actual, but not the apparent, contact angle starts to decrease as Ca increases. This is because the surface layer density at the liquid/vapour interface starts to increase significantly as Ca increases, which implies a reduction in surface tension there, and hence a decrease in the contact angle. These results emphasize, firstly, that the effect of viscous bending, which leads to the difference between the actual and apparent contact angles, becomes more important as λ decreases, and secondly, that the results start to look more like real experimental data for lower values of λ. Indeed, we note that our earlier estimate of the size of λ was 2.5.

Figures 8 to 10 show the effect of varying the dimensionless parameters, ρ_{es}, K and Ca_0^i, with $\lambda = 1$ in each case. The solution is less sensitive to changes in A and Ca_0. The ratio of the equilibrium surface densities, ρ_{es}, strongly affects the behaviour of the microscopic contact angle, θ_c. For low values of ρ_{es}, θ_c decreases rapidly, and we were unable to obtain a converged solution for relatively small values of Ca. The parameter K, which affects the separation of scales between inner, slip and outer regions, modifies the rate at which θ_c changes with Ca. The parameter Ca_0^i, which determines the strength of the flow through the contact line, also affects the behaviour of θ_c. Note that the apparent contact angle is rather insensitive to changes in any parameter other than λ, which suggests that this particular flow is well-suited neither to the task of distinguishing between Shikhmurzaev's theory and others, nor to extracting estimates of the physical parameters needed for the theory. In § 6, we discuss another experimental set up that may be better suited to testing the theory. Nonetheless, we will soldier on, and make a comparison with some experimental data.

https://doi.org/10.1017/S0956792506006589 Published online by Cambridge University Press

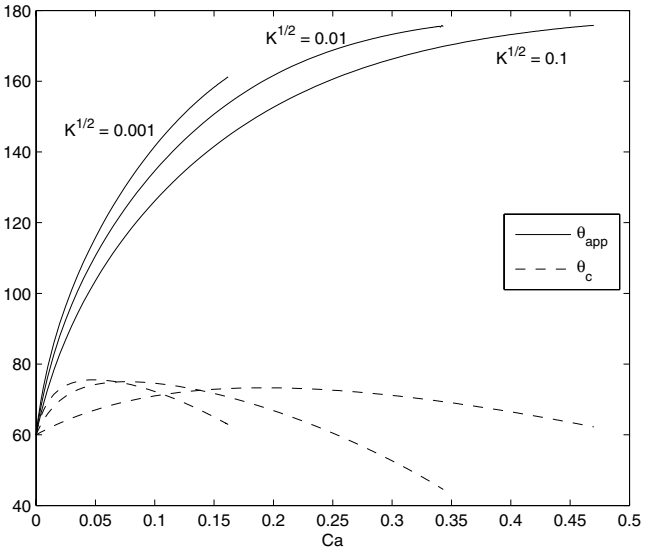


FIGURE 9. The microscopic and apparent contact angles, plotted for various values of K. In each case, the apparent contact angle is larger than the microscopic contact angle.

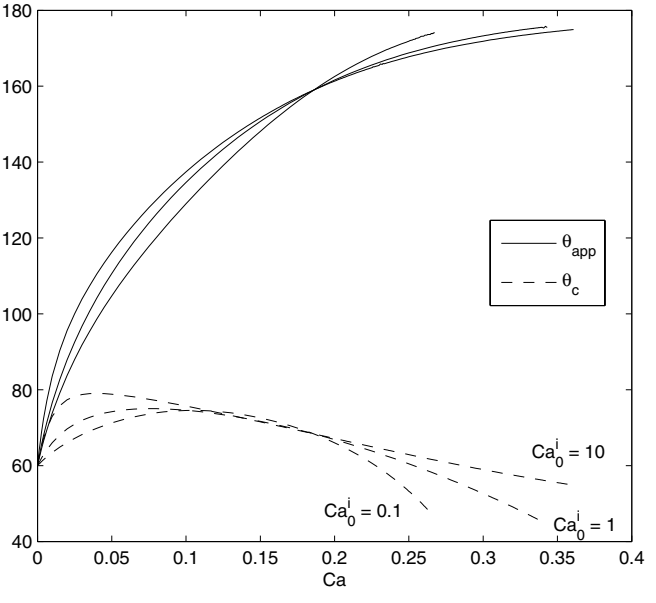


FIGURE 10. The microscopic and apparent contact angles, plotted for various values of Ca_0^i. In each case, the apparent contact angle is larger than the microscopic contact angle.

5 Comparison with experiment

We will now consider how our modified version of the theory compares with the experimental data presented by Blake and Shikhmurzaev [11]. This data relates to nine sets of

https://doi.org/10.1017/S0956792506006589 Published online by Cambridge University Press

Table 3. *The viscosity of the nine different glycerol/water solutions*

Percentage of glycerol	95%	86%	80%	72%	68%	59%	43%	16%	0%
Viscosity (mPa s)	672	104	58	23	19	10	4.2	1.5	1

experiments that measured the variation of dynamic contact angle with contact line speed for a smooth polyetheleneterephthalate (PET) tape plunging into a container that held water/glycerol solutions of various concentrations. Each of these fluids had roughly the same surface tension and static contact angle, but varied over three orders of magnitude in viscosity (see table 3). For more details on these data sets and the experimental set up, see Shikhmurzaev [11]. These data sets contain many more points than those of most other investigators [34], and also cover the variation of the apparent contact angle up to 180°, when air is entrained into the liquid. The steady, small capillary number Stokes flow that we have been analysing occurs close to the contact line in these experiments. We should also note that when the static contact angle is sufficiently small, we are unable to obtain a converged numerical solution, which rules out, for now, several other available data sets. The problem of thin film flow using Shikhmurzaev's theory is discussed elsewhere [8].

Blake and Shikhmurzaev were able to fit Shikhmurzaev's analysis of his theory to their experimental data, neglecting the effect of viscous bending, using a single set of parameters for all nine fluids, with the differences in the values of Ca at which the measured contact angle reaches 180° due solely to the difference in relative viscosity between the fluid and the surrounding air.

As discussed in Shikhmurzaev [11], the flow at small capillary number, less than around 1.5×10^{-3}, was unsteady, and it seems likely that some additional physics needs to be invoked at the contact line [30]. We therefore concentrate on the data for $\mathrm{Ca} > 1.5\times10^{-3}$. Figure 11 shows the measured (apparent) contact angle as a function of Ca for each of the nine data sets, labelled by the percentage of glycerol present in the fluid. For each of these fluids, the static contact angle was close to 65°, so the data shows that the apparent contact angle varies significantly from the static value even at very low capillary numbers.

The apparent contact angles lie close to each other until this angle becomes close enough to 180^o that the viscosity of the air becomes significant, when there is a rapid increase in contact angle with Ca, and eventual air entrainment. The lower the viscosity of the fluid (the lower the concentration of glycerol), the smaller the value of Ca at which this occurs.

We began our analysis by fitting a curve of the convenient form

$$\theta_{app} = 180^\circ - k_2 e^{-k_1 \mathrm{Ca}} - (180^\circ - k_2 - \theta_s)\, e^{-k_3 \mathrm{Ca}}$$

to all of the data points that were unaffected by the viscosity of the surrounding air. Note that $\theta_{app}(0) = \theta_s$ and $\theta_{app} \to 180^\circ$ as $\mathrm{Ca} \to \infty$. There is an element of subjectivity in the choice of data points that are fitted, but the resulting curve, which has $k_1 = 6.60$, $k_2 = 91.7^\circ$ and $k_3 = 864$, and is shown in Figure 11, clearly provides a reasonable fit to the data. Next, we fitted Shikhmurzaev's theory to this curve. For any given set of the 7 dimensionless parameters, $\tilde{p}_{es}$, A, s_{app}, λ, K, Ca_0 and Ca_0^i, we can generate a quick prediction of the

https://doi.org/10.1017/S0956792506006589 Published online by Cambridge University Press

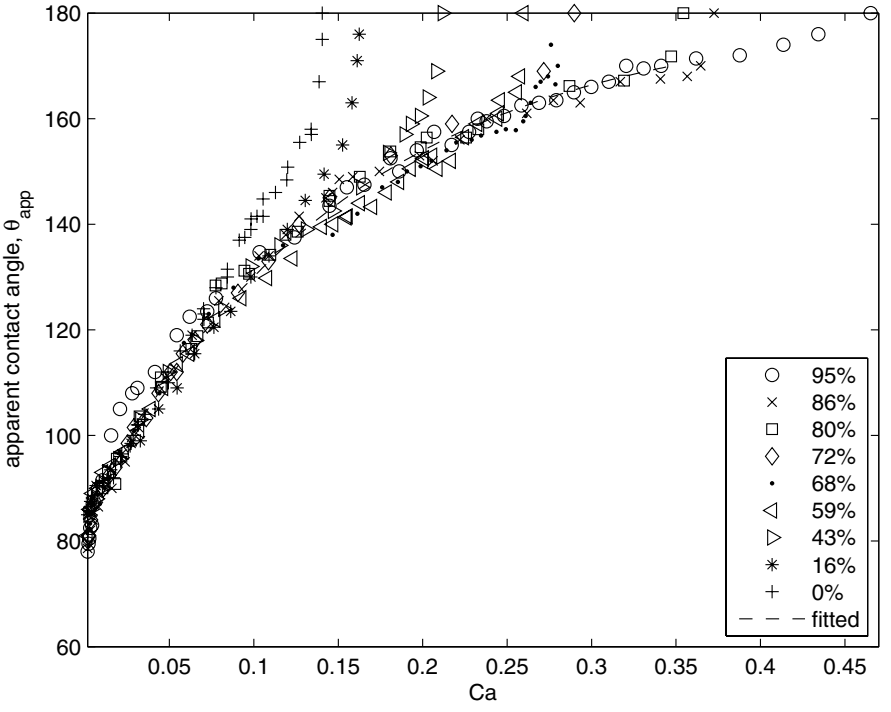


FIGURE 11. The experimental data sets of Blake and Shikhmurzaev (2002) and a curve fitted to the data for which the viscosity of the surrounding air is negligible.

variation of the apparent contact angle with Ca using our boundary integral solver for the single fluid problem with just 25 elements on each surface. Using these quick predictions we performed a least squares fit to the synthetic curve shown in 11. The best fit[9] occurs for $\tilde{\rho}_{es} = 3.10$, $A = 0.092$, $s_{app} = 130$, $\lambda = 0.12$, $K^{1/2} = 4.7 \times 10^{-3}$, $\mathrm{Ca}_0 = 0$ and $\mathrm{Ca}_0^i = 0.19$. We then increased the number of boundary elements to 500 and confirmed that this remains a good fit, as shown in Figure 12. Note that the value of A determined by fitting is close to the value $1/12 \approx 0.083$ suggested in Shikhmurzaev [24], based upon an analogy with channel flow. The value of λ is somewhat lower than we suggested earlier, a point that we shall return to below. The value of Ca_0^i is significantly larger than we predicted on the basis of the estimate $U_0^i = O(h/\tau)$, which remains to be explained.

Also shown in Figure 12 is the theoretical prediction of the actual contact angle, which varies rapidly until $\mathrm{Ca} = O(\lambda K^{1/2})$, and then slowly decreases. As discussed earlier, advection of the surface layer by the solid surface is only important when $\mathrm{Ca} = O(\lambda K^{1/2})$, and dominates for $\mathrm{Ca} \gg \lambda K^{1/2}$. It is clear that the majority of the variation in apparent contact angle is provided by viscous bending, which, in contrast to the analysis presented in Shikhmurzaev [11], cannot be neglected.

To study the individual data sets, we need to modify our model and numerical solution method to take into account the effect of the air outside the fluid. The modifications

[9] The best fit produced a very small value of Ca_0, and the resulting curve was indistinguishable from that with $\mathrm{Ca}_0 = 0$, so we take $\mathrm{Ca}_0 = 0$ here.

https://doi.org/10.1017/S0956792506006589 Published online by Cambridge University Press

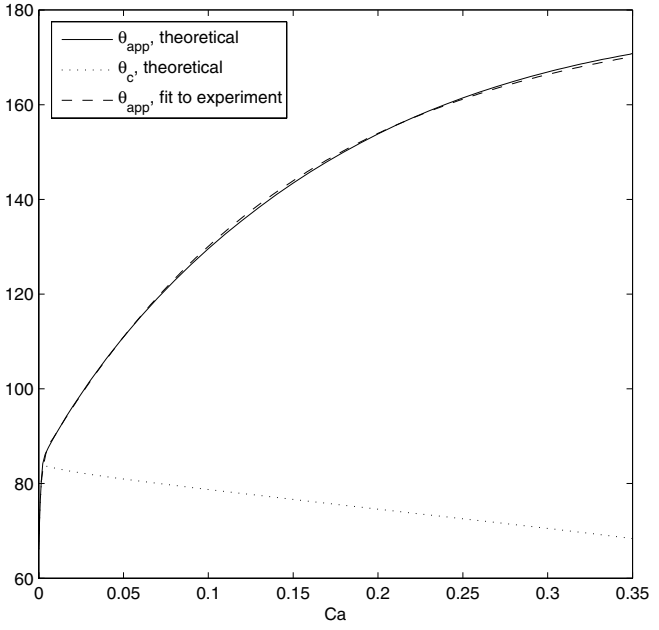


FIGURE 12. The best fit curve to the synthetic data set.

needed are discussed in Appendix B. For each data set, we used the best fit parameters calculated above, along with the known fluid/air viscosity ratio. The results are shown in Figure 13. Whilst not perfect, the trend in the value of Ca at which the surrounding air starts to affect the solution is correctly predicted. As we noted earlier, our numerical method does not cope well with thin layers of fluid, and therefore does not provide us with a solution for values of θ_{app} close to 180^o. However, the value of Ca at which the theoretical predictions end in Figure 13 indicates where the air begins to have a significant effect.

Using the known values of the surface tension, viscosity and density of the fluid, along with the fact that the apparent contact angle was measured a distance 2×10^{-5} m from the contact line in the experiments, we can deduce the values of the physical parameters. In particular, $\tau/\mu \approx 4.2 \times 10^{-3}\,\mathrm{kg^{-1}\,m^{-1}\,s^2}$, which the theory predicts to be independent of μ. This is significantly larger than the prediction made in Shikhmurzaev [11], of $3.7 \times 10^{-6}\,\mathrm{kg^{-1}\,m^{-1}\,s^2} < \tau/\mu < 1.3 \times 10^{-5}\,\mathrm{kg^{-1}\,m^{-1}\,s^2}$. Also, $\gamma \approx 7.8 \times 10^4\,\mathrm{m^2\,s^{-2}}$, rather lower than the value for the bulk fluid. The lengthscales for the inner, slip and outer regions are 7.2×10^{-10} m, 1.55×10^{-7} m and 3.21×10^{-5} m, respectively.

6 Conclusions

In this paper, we have shown that the theory for the motion of a contact line along a solid surface first presented in Shikhmurzaev [24], is incomplete. Although the theory has many attractive features, a careful analysis of its application to steady Stokes flow with strong surface tension reveals that there is a one-parameter family of asymptotic solutions, and that the original analysis implicitly uses the requirement that there should

https://doi.org/10.1017/S0956792506006589 Published online by Cambridge University Press

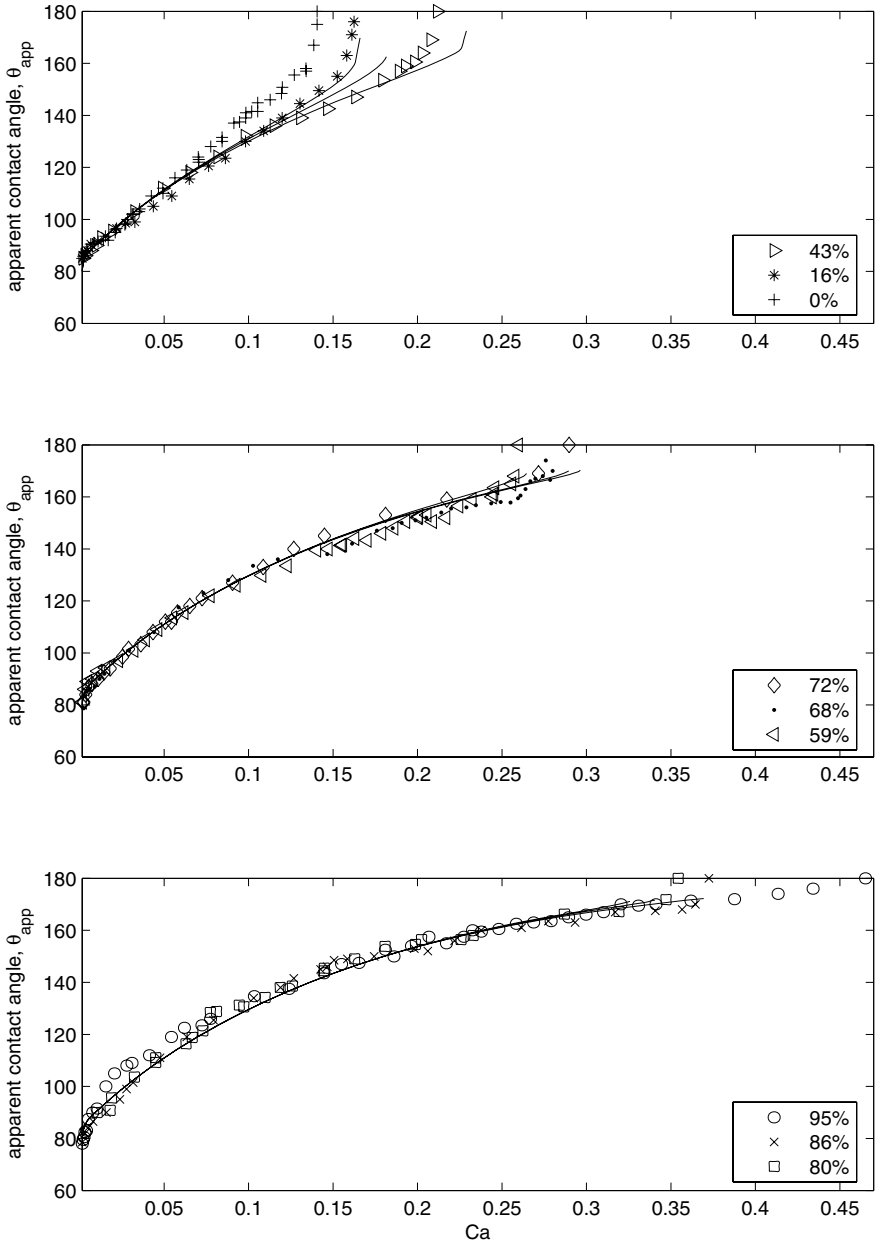


FIGURE 13. The best fit curves to the experimental data sets (solid lines).

be just two, rather than three, asymptotic regions. By considering the thermodynamics of the contact line, Bedeaux [4], has shown that there is an additional condition that relates the flux through the contact line to the chemical potentials at the interfaces, and hence to the deviation of the surface densities from equilibrium [4]. This leads to a linear relationship between the cosine of the contact angle and the contact line velocity when the surface layers are assumed to be almost incompressible. We find that, in order to fit

https://doi.org/10.1017/S0956792506006589 Published online by Cambridge University Press

the corrected theory to the experimental data of Blake & Shikmurzaev [11], we need to assume that the surface layers are compressible, and take into account the effect of both viscous bending and the viscosity of the surrounding air. A reasonable fit is then possible.

Our results show that fitting the theoretical predictions to experimental data for Stokes flow at low capillary number is now rather less convincing than fits based on the original analysis presented in Shikhmurzaev [24, 27]. After all, we now have seven parameters with which to fit to the data, two of which (λ and Ca_0^i) appear to take unexpectedly small and large values, respectively. In particular, the low value of λ, and hence the unexpectedly high compressibility of the surface layers, suggests that the assumption of a linear relationship between surface layer density and surface tension, (2.2), is probably incorrect, and that, although this cannot help but introduce extra parameters, a nonlinear relationship should be used (see also Shikhmurzaev [31] for a discussion of the form of this relationship). This also suggests that the linear equations (2.23) and (2.24), which relate the flux of fluid through the contact line to the difference in chemical potential, should be nonlinear.

As noted earlier, steady viscous flow is not an ideal experimental configuration with which to test any theory for the motion of a contact line, because of the experimental difficulty of resolving the position of the free surface at lengthscales below that of visible light, and also because viscous bending dominates the deformation of the surface close to the contact line. The timescale τ is a feature of Shikhmurzaev's theory that is not present in other theories. This suggests that an experiment involving an unsteady flow that varies on this timescale could be used to distinguish Shikhmurzaev's theory from other theories. For example, a droplet could be placed on a smooth solid surface, which could then be driven by piezo-electric means to vibrate at MHz frequencies to access timescales down to 10^{-6} s. It may well be that the global features of this flow are significantly different for Shikhmurzaev's theory compared to other theories. This is pure speculation at present, but I plan to attempt an analysis of some simple oscillatory flows in the near future. Note that in Hocking [15] something similar was done for a system with Navier slip at the solid surface and a constant, small contact angle. Studies of similar inviscid, oscilatory systems with moving contact lines can be found in Billingham [7] and Lyubimov *et al.* [18]. Repeating any of these calculations using Shikhmurzaev's theory will be technically very challenging.

Acknowledgements

I would like to thank Yulii Shikhmurzaev for many lively discussions, but note that we disagree on almost every aspect of the analysis and conclusions presented here. I am also grateful to Dick Bedeaux for providing the missing boundary condition and to Terry Blake for many helpful discussions and for providing me with the experimental data discussed in section 5. This work was made possible by an EPSRC Advanced Research Fellowship.

Appendix A The homogeneous boundary value problem in the outer asymptotic region

Consider the boundary value problem given by (3.39) to (3.42). The only parameter is θ_c, the angle of the wedge. We will solve this problem using Mellin integral transforms. We

https://doi.org/10.1017/S0956792506006589 Published online by Cambridge University Press

define the Mellin transform of Ψ to be

$$\bar{\Psi}(s,\theta) = \int_0^\infty r^{s-1}\Psi(r,\theta)dr, \tag{A 1}$$

dropping the hats on r for notational convenience. A coordinate expansion shows that $\Psi = O(r)$ for $r \ll 1$. Since we also have $\Psi \to 0$ as $r \to \infty$, we know that

$$\bar{\Psi}(s,\theta) \text{ is analytic for } -1 \leqslant \mathrm{Re}(s) < 0, \text{ except for a simple pole at } s = -1. \tag{A 2}$$

It is straightforward to show that the Mellin transform of a solution of the biharmonic equation, (3.39), is

$$\bar{\Psi}(s,\theta) = A(s)\sin s\theta + B(s)\cos s\theta + C(s)\sin(s+2)\theta + D(s)\cos(s+2)\theta,$$

for some functions $A(s)$, $B(s)$, $C(s)$ and $D(s)$. On applying the simpler of the three boundary conditions, we find that we can write

$$\bar{\Psi}(s,\theta) = K(s)G(s,\theta), \tag{A 3}$$

where

$$G(s,\theta) = \left\{\frac{(s+2)\sin s\theta - s\sin s\theta}{(s+2)\sin s\theta_c - s\sin s\theta_c}\right\} - \left\{\frac{\cos s\theta - \cos(s+2)\theta}{\cos s\theta_c - \cos(s+2)\theta_c}\right\}. \tag{A 4}$$

Applying the final boundary condition shows that $K(s)$ satisfies the functional difference equation

$$K(s) = F(s)K(s-1), \tag{A 5}$$

where,

$$\begin{aligned} F(s) = s(s+1)&\left\{(s^2-1)\frac{\cos(s-1)\theta_c - \cos(s+1)\theta_c}{(s+1)\sin(s-1)\theta_c - (s-1)\sin(s+1)\theta_c}\right. \\ &\left. + \frac{(s-1)\sin(s-1)\theta_c - (s+1)\sin(s+1)\theta_c}{\cos(s-1)\theta_c - \cos(s+1)\theta_c}\right\} \\ &\Big/\left\{-s(s+2)\frac{s\sin s\theta_c - (s+2)\sin(s+2)\theta_c}{(s+2)\sin s\theta_c - s\sin(s+2)\theta_c} + \frac{s^2\cos s\theta_c - (s+2)^2\cos(s+2)\theta_c}{\cos s\theta_c - \cos(s+2)\theta_c}\right\}. \end{aligned} \tag{A 6}$$

Before we solve (A 5), note that $G(s,\theta)$ is bounded for $-1 \leqslant \mathrm{Re}(s) \leqslant 0$, and nonzero at $s = -1$, so that, using (A 2),

$$K(s) \text{ is analytic for } -1 \leqslant \mathrm{Re}(s) < 0, \text{ except for a simple pole at } s = -1. \tag{A 7}$$

Let's begin by considering what happens in a slender wedge, for which $\theta_c \ll 1$. In this case, we find that

$$G(s,\theta) \sim \frac{\theta^2}{\theta_c^2}\left(1 - \frac{\theta}{\theta_c}\right), \quad F(s) \sim \frac{1}{4}s(s+1)\theta_c.$$

https://doi.org/10.1017/S0956792506006589 Published online by Cambridge University Press

For $\theta_c \ll 1$, the solution of (A 5) that satisfies (A 7) and decays rapidly enough as $s \to \pm i\infty$ that the inverse Mellin transform exists is therefore

$$\bar{\Psi}(s,\theta) = k_0 \left(\frac{1}{4}\theta_c\right)^s \Gamma(s+1)\Gamma(s+2)\theta^2(\theta_c - \theta),$$

for some arbitrary constant k_0. Note that this function has a simple pole at $s = -1$, double poles at $s = -2, -3, \ldots$, and is analytic for $\mathrm{Re}(s) > -1$. This is consistent with the coordinate expansion (3.43), and also shows that Ψ decays to zero exponentially fast as $r \to \infty$. Moreover, this is the Mellin transform of a known function, with the correct behaviour for large and small r, namely

$$\Psi = \Psi_0\, \theta^2(\theta_c - \theta) r^{3/2} K_1\left(4\sqrt{\frac{r}{\theta_c}}\right), \tag{A 8}$$

for some arbitrary constant Ψ_0. We can verify that this is the correct solution by noting that, for $\theta_c \ll 1$, the biharmonic equation becomes, at leading order, $\partial^4\Psi/\partial\theta^4 = 0$. Therefore,

$$\Psi(r,\theta) \sim \theta^2(\theta_c - \theta) f(r),$$

and the second of the boundary conditions (3.41) gives

$$\frac{d^2}{dr^2}\left(\frac{\theta_c}{r} f\right) - \frac{4}{r^2} f = 0.$$

The bounded solution of this equation then leads to (A 8).

To solve (A 5) for general θ_c, we use a method described in the appendix to Atkinson & Craster [1], based on treating (A 5) as a Riemann-Hilbert problem. Firstly, we need to note that

$$F(s) = \pm\frac{1}{2} i(s+1)\left\{1 + O(|s|^{-2})\right\} \quad \text{as } s \to \pm i\infty.$$

We now seek to solve the two separate functional difference equations,

$$\hat{K}(s) = \frac{1}{2}(s+1)\tan \pi s\, \hat{K}(s-1), \tag{A 9}$$

and

$$\bar{K}(s) = \bar{F}(s)\bar{K}(s-1), \tag{A 10}$$

where

$$\bar{F}(s) = \frac{2}{(s+1)\tan \pi s} F(s).$$

The point of this is that $\hat{K}(s)\bar{K}(s)$ is a solution of (A 5), and that $\bar{F}(s)$ has been defined so that

$$\bar{F}(s) = 1 + O(|s|^{-2}) \quad \text{as } s \to \pm i\infty,$$

which will be crucial later.

https://doi.org/10.1017/S0956792506006589 Published online by Cambridge University Press

By inspection, a solution of (A 9) is

$$\hat{K}(s) = 2^{-s}\Gamma(s+2)\frac{G\left(\frac{3}{2}-s,1\right)G\left(\frac{3}{2}+s,1\right)}{G(2-s,1)\,G(1+s,1)}, \tag{A 11}$$

where $G(z,\delta)$ is the Barnes double gamma function [2], which gives a convenient representation of the solution of functional difference equations that involve products of trigonometric functions [16]. The Barnes double gamma function is defined to be the solution of the functional difference equation

$$G(z+1,\delta) = \Gamma(z/\delta)G(z,\delta),$$

subject to the normalization condition, $G(1,\delta) = 1$. An integral representation for the Barnes double gamma function that allows it to be computed in a straightforward manner is given in Lawrie & King [16], and asymptotic expansions in various limits are derived in Billingham & King [6]. Now, since $G(z,1)$ has zeros at $z = 0,-1,-2,\ldots$ and no poles, $\hat{K}(s)$ is analytic for $-1 \leqslant \mathrm{Re}(s) < 0$, except for a simple pole at $s = -1$.

Using the method described in Atkinson & Craster [1], the unique solution of (A 10) that has $\bar{K}(s) \to 1$ as $|s| \to \infty$ is

$$\bar{K}(s) = \exp\left\{\frac{1}{2i}\int_{-i\infty}^{i\infty}\cot\pi(t-s)\log\bar{F}(t)\,dt\right\}, \tag{A 12}$$

for $-1 \leqslant \mathrm{Re}(s) < 0$. After analysing the behaviour of the gamma functions and Barnes double gamma functions for s large and imaginary, we find that the solution of the original functional difference equation, (A 5), that is analytic for $-1 \leqslant \mathrm{Re}(s) < 0$, except for a simple pole at $s = -1$, and decays rapidly enough as $s \to \pm i\infty$ that the Mellin inversion integral converges, is

$$K(s) = k_0 2^{-s}\Gamma(s+2)\frac{G\left(\frac{3}{2}-s,1\right)G\left(\frac{3}{2}+s,1\right)}{G(2-s,1)\,G(1+s,1)} \times \exp\left\{\frac{1}{2i}\int_{-i\infty}^{i\infty}\cot\pi(t-s)\log\bar{F}(t)\,dt\right\}, \tag{A 13}$$

with k_0 an arbitrary constant.

We now need to determine the pole structure of the solution to which this corresponds outside the strip $-1 \leqslant \mathrm{Re}(s) < 0$ to find out how Ψ behaves for large and small r. Now that we know $K(s)$ in this strip, we can simply use the original functional difference equation (A 5), to determine $K(s)$ elsewhere. It is clear that the location of the poles and zeros of $F(s)$ will be crucial.

A zero of $F(s)$ at $s = s_0$ with $\mathrm{Re}(s_0) < 0$ corresponds to poles of $K(s)$ at $s = s_0 - n$, $n = 1,2,\ldots$. It is clear from the definition, (A 6), of $F(s)$ that it has zeros at $s = 0$ and $s = -1$. The zero at $s = 0$ has already been taken into account (in effect it generates the simple pole at $s = -1$), but the zero at $s = -1$ leads to double poles at $s = -2,-3,\ldots$, ignoring the effect of any other possible zeros for the moment. This will generate a coordinate expansion of the form (3.43), as required. If $F(s)$ has a zero with $-1 < \mathrm{Re}(s) < 0$, the coordinate expansion (3.43) will not be valid, and the asymptotic structure that we have constructed will not work. Although we have not been able to prove this, a numerical investigation of $F(s)$ indicates that no such zero exists.

https://doi.org/10.1017/S0956792506006589 Published online by Cambridge University Press

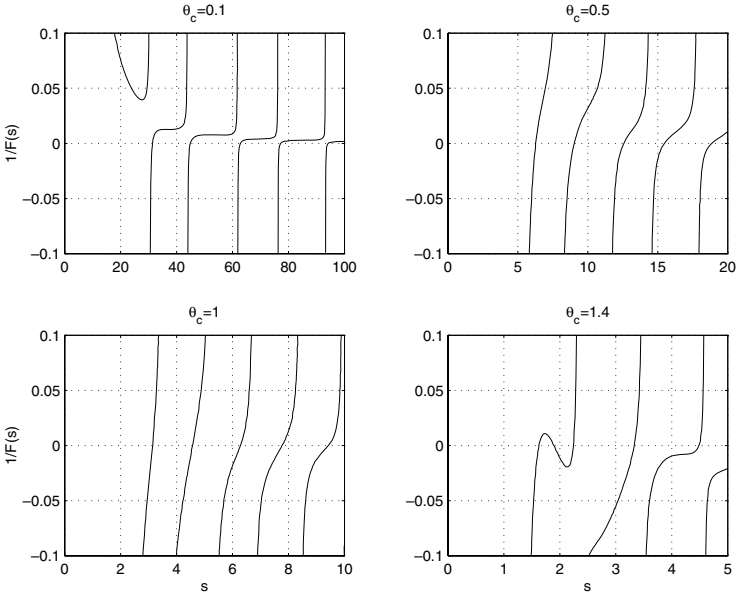


FIGURE A 1. The function $1/F(s)$ for real, positive s when $\theta_c = 0.1$, 0.5, 1 and 1.4.

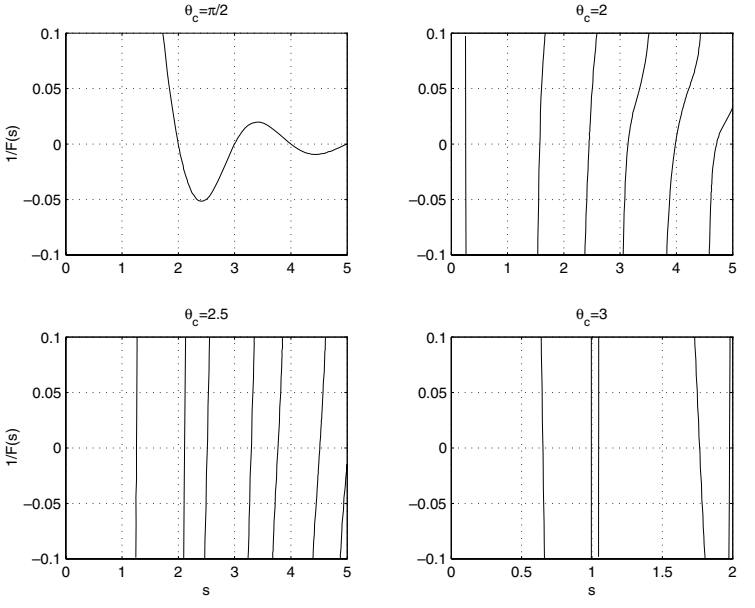


FIGURE A 2. The function $1/F(s)$ for real, positive s when $\theta_c = \pi/2$, 2, 2.5 and 3.

A pole of $F(s)$ at $s = s_1$ with $\mathrm{Re}(s_1) > 0$ corresponds to poles of $K(s)$ at $s = s_1 + m$, $m = 0, 1, 2, \ldots$. Therefore, we can investigate how Ψ behaves as $r \to \infty$ by determining the pole of $F(s)$ with smallest real part in $\mathrm{Re}(s) > 0$. Starting with the real axis, Figures A 1 and A 2 show that $F(s)$ has poles (zeros of $1/F(s)$ in the figures) that approach the origin as θ_c increases. This shows that, although at leading order the decay of Ψ as $r \to \infty$

https://doi.org/10.1017/S0956792506006589 Published online by Cambridge University Press

is exponential when $\theta_c \ll 1$, in general this decay is algebraic with the rate of decay decreasing as θ_c increases, at least for $0 \leqslant \theta_c \leqslant \pi/2$. Further numerical investigation of $|F(s)|$ suggests that, although there may be off-axis poles, they do not greatly affect the rate of decay as $r \to \infty$.

In conclusion, although we have not investigated what the solutions look like (this would involve evaluating numerically a double integral, one in (A 13), and one in the Mellin inversion formula, for each value of r and θ, which is a very tough proposition), we have shown that they exist by constructing an explicit formula for them. The key point is that (A 13) gives the correct pole structure *and* decays rapidly enough as $s \to \pm\infty$ that the Mellin inversion integral exists.

Appendix B The two fluid problem

The analysis of a fluid/fluid contact line presented in Shikhmurzaev [27] is based on the assumption that the interface between two fluids can be modelled using two surface layers, with densities ρ^i_{sk} and velocities v^i_{sk}, where $k = 1,2$ for the two fluids. After eliminating these surface layer velocities, as we did in the main part of the paper, we arrive at the steady surface layer equations

$$\alpha_k\gamma_k \frac{d}{ds_i}\left(\rho^i_{sk}\frac{d\rho^i_{sk}}{ds_i}\right) - \frac{1}{2}\frac{d}{ds_i}\left\{\rho^i_{sk}\left(u^i_{sk}+U^i\right)\right\} - \frac{\rho^i_{sk}-\rho^i_{esk}}{\tau_k} = 0, \tag{B 1}$$

$$\beta_k\left(u^i_{sk}-U^i\right) = \mathbf{f}^i_k\cdot\mathbf{t}^i - \frac{1}{2}\gamma_k\frac{d\rho^i_{sk}}{ds_i}, \tag{B 2}$$

in each layer, coupled by the stress continuity conditions

$$\mathbf{f}^i_1\cdot\mathbf{t}^i + \mathbf{f}^i_2\cdot\mathbf{t}^i = \gamma_1\frac{d\rho^i_{s1}}{ds_i} + \gamma_2\frac{d\rho^i_{s2}}{ds_i}, \tag{B 3}$$

$$\mathbf{f}^i_1\cdot\mathbf{n}_1 + \mathbf{f}^i_2\cdot\mathbf{n}_2 = \left\{\gamma_1\left(\rho^i_{s1}-\rho^i_{01}\right) + \gamma_2\left(\rho^i_{s2}-\rho^i_{02}\right)\right\}\kappa, \tag{B 4}$$

where U^i is the velocity at the interface between the two layers and $\mathbf{t}^i$ is the tangent to the interface. We can use (B 2) to eliminate U^i from (B 1), which gives two nonlinear diffusion equations for ρ^i_{sk}. Boundary conditions at infinity and at the contact line analogous to (2.21), (2.22) and (2.24), along with surface layer equations on the solid surface in each fluid then close the system.

Note that in Shikhmurzaev [27] it is stated that conservation of angular momentum at the interface between the fluids leads to

$$\gamma_1\frac{d\rho^i_{s1}}{ds_i} = \gamma_2\frac{d\rho^i_{s2}}{ds_i}. \tag{B 5}$$

This equation is incorrect, and not needed. Conservation of angular momentum is expressed through the symmetry of the stress tensor in the fluid layers (although this does not appear explicitly), and not through (B 5). Moreover, it is clear that, if (B 5) holds, the surface layer densities are linearly related through $\gamma_1(\rho^i_{s1}-\rho^i_{es1}) = \gamma_2(\rho^i_{s2}-\rho^i_{es2})$. There is then no way to satisfy the two independent nonlinear equations that govern ρ^i_{sk}. This is

https://doi.org/10.1017/S0956792506006589 Published online by Cambridge University Press

not immediately obvious in Shikhmurzaev [27], since the equilibrium solution $\rho^i_{sk} = \rho^i_{esk}$ is used throughout the analysis.

We can recover the equations for a liquid/air system by neglecting all of the surface layer densities in fluid 2 relative to those in fluid 1, and the interfacial stresses in fluid 2 relative to those in fluid 1 ($\mu_2 \ll \mu_1$). However, when the air forms a sufficiently thin layer, the interfacial shear stress due to the flow in the air will not be negligible, and we retain this. As we might expect, (2.14) becomes, retaining the subscripts on fluid 2 quantities only,

$$\mathbf{f}^i \cdot \mathbf{t}^i + \mathbf{f}^i_2 \cdot \mathbf{t}^i = \gamma \frac{d\rho^i_s}{ds_i}, \tag{B 6}$$

whilst (2.13) becomes

$$\frac{\gamma\alpha(1+4A)}{4A}\frac{d}{ds_i}\left(\rho^i_s \frac{d\rho^i_s}{ds_i}\right) - \frac{d}{ds_i}\left\{\rho^i_s\left(u^i_s + \frac{1}{2\beta}\mathbf{f}^i_2 \cdot \mathbf{t}^i\right)\right\} - \frac{\rho^i_s - \rho^i_{es}}{\tau} = 0, \tag{B 7}$$

which now contains the shear stress due to the air, $\mathbf{f}^i_2 \cdot \mathbf{t}^i$.

At the interface, the tangential velocity of the air is coupled to that in the fluid through the slip relation

$$u^i_{s2} = u^i_s + \frac{1}{\beta_2}\mathbf{f}^i_2 \cdot \mathbf{t}^i - \frac{1}{\beta}\mathbf{f}^i \cdot \mathbf{t}^i + \frac{\gamma}{2\beta}\frac{d\rho^i_s}{ds_i}. \tag{B 8}$$

On the solid surface in contact with the air, we have the Navier slip condition

$$u_{s2} = U - \frac{1}{\beta_2}\mathbf{f}_2 \cdot \mathbf{t}. \tag{B 9}$$

We modified our numerical solution method to include the boundary integral solution for Stokes flow in the air, coupled to the flow in the fluid through (B 6), (B 8) and (B 9), taking $\beta_2 = \mu_2\beta/\mu\hat{h}_2$. Here, $\hat{h}_2$ is the ratio of the mean free path in air, which we use as an estimate of the surface layer thickness and took to be 3×10^{-7}m, and the inner lengthscale, $K^{1/2}L$. For the best fit discussed in the text, $\hat{h}_2 \approx 400$.

References

[1] Atkinson, C. & Craster, R. V. (1994) Interfacial fracture of a radially inhomogeneous elastic bimaterial. *Int. J. Solids Structures* **31**, 1207–1223.

[2] Barnes, E. W. (1899) The genesis of the double gamma function. *Proc. Lond. Math. Soc.* **31**, 358–381.

[3] Bedeaux, D., Albano, A. M. & Mazur P. (1976) Boundary conditions and non-equilibrium thermodynamics. *Physica A* **82**, 438–462.

[4] Bedeaux, D. (2003) Nonequilibrium thermodynamic description of the three phase contact line. *J. Chem. Phys.* **120**, 3744–3748.

[5] Billingham, J. (1997) The unsteady motion of three phase contact lines. In *IUTAM Symposium on Nonlinear Singularities in Deformation and Flow*, Durban, D. & Pearson, J. R. A. *eds.*

[6] Billingham, J. & King, A. C. (1997) Uniform asymptotic expansions for the Barnes double gamma function. *Proc. R. Soc. Lond. A* **453**, 1817–1829.

[7] Billingham, J. (2002) Nonlinear sloshing in zero gravity. *J. Fluid Mech.* **464**, 365–391.

https://doi.org/10.1017/S0956792506006589 Published online by Cambridge University Press

[8] Billingham, J. (2006) Gravity-driven thin film flow using a new contact line model. Submitted to *IMA J. Appl. Math.*
[9] Blake, T. D., Dobson, R. A. & Ruschak, K. J. (2004) Wetting at high capillary numbers. *J. Coll. Int. Sci.* **279**, 198–205.
[10] Blake, T. D., Bracke, M. & Shikhmurzaev, Y. D. (1999) Experimental evidence of nonlocal hydrodynamic influence on the dynamic contact angle. *Phys. Fluids* **11**, 1995–2007.
[11] Blake, T. D. & Shikhmurzaev, Y. D. (2002) Dynamic wetting by liquids of different viscosity. Blake, *J. Coll. Int. Sci.* **253**, 196–202.
[12] Cox, R. G. (1986) The dynamics of spreading of liquids on a solid surface. Part 1. Viscous flow. *J. Fluid Mech.*, **168**, 169–194.
[13] Dussan V., E. B. & Davis, S. H. (1974) On the motion of a fluid-fluid interface along a solid surface. *J. Fluid Mech.*, **65**, 71–95.
[14] Eggers, J. & Evans, R. (2004) Comment on "Dynamic wetting by liquids of different viscosity," by T.D. Blake & Y.D. Shikhmurzaev. *J. Coll. Int. Sci.*, **280**, 537–538.
[15] Hocking, L.M. (2003) Contact angles and inertia for liquid bounded by an oscillating plate. *Q. J. Mech. Appl. Math.*, **56**, 271–288.
[16] Lawrie, J. B. & King, A.C. (1994) Exact solution to a class of functional difference equations with application to a moving contact line flow. *Euro. J. Appl. Math.* **5**, 141–157.
[17] Lindner-Silwester, T. & Schneider, W. (2005) The moving contact line with weak viscosity effects - an application and evaluation of Shikhmurzaev's model. *Acta Mech.* **176**, 245–258.
[18] Lyubimov, D. V., Lyubimova, T. P. & Shklyaev, S. V. (2006) Behaviour of a drop on an oscillating solid plate. *Phys. Fluids*, **18**, art. 012101.
[19] Moffatt, H. K. (1964) Viscous and resistive eddies near a sharp corner. *J. Fluid Mech.*, **18**, 1–18.
[20] Monnier, J. & Witomski, P. 2004 Analysis of a local hydrodynamic model with Marangoni effect. *J. Sci. Comp.*, **21**, 369–403.
[21] Pomeau, Y. (2002) Recent progress in the moving contact line problem. *C. R. Mecanique*, **330**, 207–222.
[22] Pozrikidis, C. (1992) *Boundary integral and singularity methods for linearized viscous flow*. Cambridge University Press.
[23] Rowlinson, J. S. & Widom, B. (1982) *Molecular Theory of Capillarity*, Oxford University Press.
[24] Shikhmurzaev, Y. D. (1993) The moving contact line on a smooth solid surface. *Int. J. Multiphase Flow* **19**, 589–610.
[25] Shikhmurzaev, Y. D. (1994) Mathematical modelling of wetting hydrodynamics. *Fluid Dyn. Res.* **13**, 45–64.
[26] Shikhmurzaev, Y. D. (1996) Dynamic contact angles and flow in vicinity of moving contact line. *AIChE Jnl.* **42**, 601–612.
[27] Shikhmurzaev, Y. D. (1997) Moving contact lines in liquid/liquid/solid systems. *J. Fluid Mech.* **359**, 313–328.
[28] Shikhmurzaev, Y. D. (1998) On cusped interfaces. *J. Fluid Mech.* **359**, 313–328.
[29] Shikhmurzaev, Y. D. (2000) Coalescence and capillary breakup of liquid volumes. *Phys. Fluids* **12**, 2386–2396.
[30] Shikhmurzaev, Y. D. (2002) On metastable regimes of dynamic wetting. *J. Phys.: Condens. Matter* **14**, 319–330.
[31] Shikhmurzaev, Y. D. (2005) Capillary breakup of liquid threads: A singularity-free solution. *IMA J. Appl. Math.* **70**, 880–907.
[32] Shikhmurzaev, Y. D. & Blake, T. D. (2004) Response to the comment on [J. Colloid Interface Sci. 253 (2002) 196] by J. Eggers & R. Evans. *J. Coll. Int. Sci.*, **280**, 539–541.
[33] Slattery, J. C. (1990) *Interfacial Transport Phenomena*, Springer-Verlag.
[34] Ström, G., Fredriksson, M., Stenius, P. & Radoev, B. (1990) Kinetics of steady wetting. *J. Coll. Int. Sci* **134**, 107–116.

https://doi.org/10.1017/S0956792506006589 Published online by Cambridge University Press